

Biophysical Analysis of Potential Inhibitors of SARS-CoV-2 Cell Recognition and Their Effect on Viral Dynamics in Different Cell Types: A Computational Prediction from In Vitro Experimental Data

Lenin González-Paz,* Carla Lossada, María Laura Hurtado-León, Joan Vera-Villalobos, José L. Paz, Yovani Marrero-Ponce, Felix Martinez-Rios, and Ysaías. J. Alvarado



Cite This: *ACS Omega* 2024, 9, 8923–8939



Read Online

ACCESS |



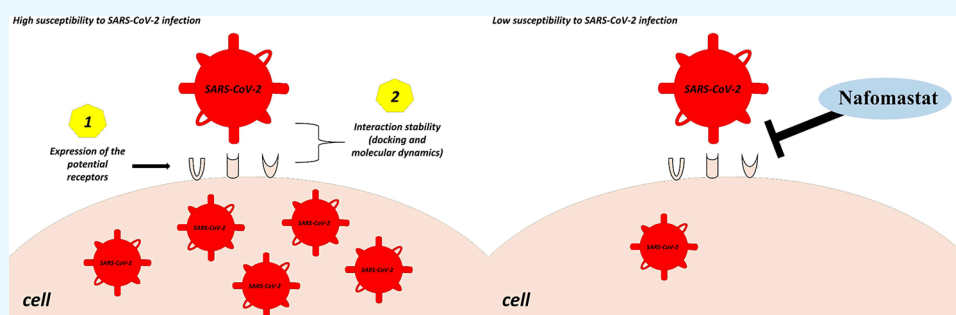
Metrics & More



Article Recommendations



Supporting Information



ABSTRACT: Recent reports have suggested that the susceptibility of cells to SARS-CoV-2 infection can be influenced by various proteins that potentially act as receptors for the virus. To investigate this further, we conducted simulations of viral dynamics using different cellular systems (Vero E6, HeLa, HEK293, and CaLu3) in the presence and absence of drugs (anthelmintic, ARBs, anticoagulant, serine protease inhibitor, antimalarials, and NSAID) that have been shown to impact cellular recognition by the spike protein based on experimental data. Our simulations revealed that the susceptibility of the simulated cell systems to SARS-CoV-2 infection was similar across all tested systems. Notably, CaLu3 cells exhibited the highest susceptibility to SARS-CoV-2 infection, potentially due to the presence of receptors other than ACE2, which may account for a significant portion of the observed susceptibility. Throughout the study, all tested compounds showed thermodynamically favorable and stable binding to the spike protein. Among the tested compounds, the anticoagulant nafomastat demonstrated the most favorable characteristics in terms of thermodynamics, kinetics, theoretical antiviral activity, and potential safety (toxicity) in relation to SARS-CoV-2 spike protein-mediated infections in the tested cell lines. This study provides mathematical and bioinformatic models that can aid in the identification of optimal cell lines for compound evaluation and detection, particularly in studies focused on repurposed drugs and their mechanisms of action. It is important to note that these observations should be experimentally validated, and this research is expected to inspire future quantitative experiments.

1. INTRODUCTION

Severe acute respiratory syndrome coronavirus 2 (SARS-CoV-2) is a single-stranded, positive-sense RNA virus that belongs to the betacoronavirus genus of the Coronaviridae family.¹ The spike protein of SARS-CoV-2 is highly conserved among human coronaviruses, including SARS-CoV-1 and MERS-CoV.¹ The spike protein is important for mediating infection by binding to host cell receptors through the receptor-binding domain (RBD).² The susceptibility of cells to the SARS-CoV-2 infection can be influenced by a variety of factors. These include the presence of proteins capable of binding to the virus, the level of expression of receptors on the host cell, and the ability of proteases to cleave the spike protein.^{2–5}

For instance, the angiotensin-converting enzyme 2 (ACE2) receptor plays a vital role in the entry of SARS-CoV-2. ACE2 is expressed in various organs, but its expression levels differ across

different human tissues. This variability in expression levels may contribute to varying levels of cellular susceptibility to SARS-CoV-2 infection.⁶ Post-translational regulation of ACE2 can occur through another potential receptor called Basigin2 (CD147). Another candidate receptor, Neuropilin 1 (NRP1), has been found to increase cell susceptibility to SARS-CoV-2 infection by enhancing the virus's infectivity. NRP1 facilitates greater viral entry into cells, rather than simply increasing the

Received: September 12, 2023

Revised: January 20, 2024

Accepted: February 5, 2024

Published: February 14, 2024



binding of the virus to the cell membrane.^{2,3} Although other potential receptors for SARS-CoV-2 have been identified, they have not been studied as extensively as ACE2. These include glucose-regulated protein 78 or heat shock protein A5 (HSPAS) angiotensin II receptor type 2 (AGTR2) and the receptor for advanced glycation end products (RAGE).³

After binding to the ACE2 receptor, the spike protein of SARS-CoV-2 must undergo proteolytic cleavage for a successful viral entry. There are several proteases that can activate SARS-CoV-2 entry, including transmembrane serine protease 2 (TMPRSS2), FURIN protease, and cysteine proteases such as L-type cathepsins (Cathepsin L).^{3,4,7} The addition of a FURIN cleavage site to the spike protein of SARS-CoV-2 is one of the key differences between this virus and the SARS-CoV-1 virus. The FURIN cleavage site makes it easier for SARS-CoV-2 to enter cells, which is one reason why this virus is more infectious than SARS-CoV-1.⁸ Interestingly, sequential passaging of SARS-CoV-2 in Vero cell lines causes a loss of the FURIN cleavage site. This results in a viral strain that is less infectious, but it is also more fit and can replicate more efficiently in cells.⁹ There has been some research suggesting that cathepsin L inhibitors could be used as therapy for COVID-19. Cathepsin L inhibitors block the activity of cathepsin L, which could prevent the cleavage of the spike protein and the entry of SARS-CoV-2 into cells. However, more research is needed to confirm the effectiveness of this approach.¹⁰

It has been reported that the presence of multiple receptors can further enhance the susceptibility of cells to infection. The SARS-CoV-2 virus can utilize various receptors, such as the ACE2 receptor and the TMPRSS2 protease, to enter cells. When multiple receptors are present, blocking the virus from entering cells becomes more challenging.³ Consequently, inhibiting only one of these proteins may not be sufficient to prevent the entry of SARS-CoV-2 into cells.⁸ Moreover, the differential expression levels of these receptors can contribute to the observed variations in the cell line susceptibility to SARS-CoV-2. For instance, certain cell lines may exhibit higher ACE2 receptor expression levels than others, rendering them more vulnerable to SARS-CoV-2 infection.^{11–13} Therefore, the choice of cell line becomes crucial when studying the infectivity of SARS-CoV-2, particularly in drug-related investigations.^{14,15}

Viral entry is the first step in the SARS-CoV-2 infectious cycle. Blocking viral entry into cells is a promising therapeutic target for COVID-19 treatment.^{16,17} Many repurposed compounds have been investigated for their ability to prevent viral entry, including the serine proteases nafamostat¹⁸ and camostat,¹⁶ the nonsteroidal inflammatory drug ibuprofen,^{19,20} the antimalarials chloroquine^{17,21} and hydroxychloroquine,¹⁷ and the ACE inhibitors captopril and telmisartan.²² The ACE inhibitors captopril and telmisartan were found to decrease ACE2 protein expression in kidney-isolated membranes. This suggests that patients taking these drugs may not need to stop treatment for the COVID-19 protection. Although these compounds act as competitive inhibitors to other host receptors, they have also been implicated in interacting with the ACE2–SARS-CoV-2 spike protein complex. This interaction may be responsible for their antiviral activity.²³

To gain a deeper understanding of the viral particle's biological cycle, researchers have proposed predictive mathematical models. These models not only describe the dynamics of various viral infections but also simulate the effectiveness of potential repurposed drugs against the virus.²⁴ In this study, we employed well-established and recommended mathematical

models to investigate viral dynamics. By utilizing data obtained from in vitro assays involving different cell lines, we calculated parameters associated with the SARS-CoV-2 viral infection. This approach allowed us to model and predict the potential efficacy of different drugs, taking into account the specific cell type.^{15,24–27} In our study, we focused on considering the expression values that are deemed more favorable for the most relevant proteins, namely, NRP1, CD147, FURIN, TMPRSS2, and ACE2.^{2–4,6,7,28} Additionally, we also considered other less studied proteins, such as HSPAS, AGTR2, RAGE, and Cathepsin-L.^{3,8,29} These evaluations were conducted using recommended cell lines for SARS-CoV-2 research, including Vero E6, HEK293T, and Calu-3.^{2,14,15,30–32} As a negative control, we selected the HeLa cell line, which is not recommended for SARS-CoV-2 research.³⁰

The objective of this research is to forecast the vulnerability of different cell lines employed in in vitro assays to SARS-CoV-2. This is accomplished through theoretical modeling of the expression patterns of a cluster of proteins known to serve as potential receptors for the virus.³ Additionally, we simulate the infection of these cells under both drug-treated and untreated conditions, aiming to inhibit the virus's binding to its receptors.^{16,17,22,23} Our primary aim of this work is to contribute to the advancement of suitable cellular models for in vitro replication assays of SARS-CoV-2.

2. MATERIALS AND METHODS

2.1. Search for Cell Lines and Proteins in Databases.

Based on a comprehensive analysis of multiple studies,^{2,14,15,31,32} we carefully selected the following cell lines for our SARS-CoV-2 research. To identify these cell lines, we utilized the “browser by cell line group” feature of the Cellosaurus server, developed by Amos Bairoch of the CALIPHO group at SIB - Swiss Bioinformatics Institute [https://web.expasy.org/cellosaurus/browse_by_group]. First, we chose the Vero E6 cell line, derived from African green monkey kidney epithelial cells, as it is specifically recommended by Cellosaurus for culturing SARS-CoV-2. In addition, we included the HEK293 cell line, derived from human embryonic kidney cells, and the CaLu3 cell line, derived from human epithelial cells found in lung adenocarcinoma. Cellosaurus designates these cell lines as valuable for investigating SARS-CoV-2. Furthermore, we incorporated the CaLu3 cell line due to its high expression levels of most of the receptors considered in this study, as indicated by the Human Protein Atlas database. This added perspective enhances the comprehensiveness of our analysis. Lastly, we included the HeLa cell line, derived from human cervix - cervical adenocarcinoma, as a control. Cellosaurus classifies this cell line as unsuitable for culturing SARS-CoV-2 [<https://web.expasy.org/cellosaurus/sars-cov-2.html>].³⁰

In order to identify the proteins that could potentially act as receptors for SARS-CoV-2, we conducted an extensive analysis of various studies.^{2–5} Additionally, we examined the presence and expression levels of a total of nine proteins associated with SARS-CoV-2 infection using data from the Human Protein Atlas database [<https://www.proteinatlas.org/>]. Specifically, we focused on five proteins that have been identified as particularly significant in this context: NRP1, CD147, FURIN, TMPRSS2, and ACE2.^{2–5,28} Furthermore, we considered four less extensively studied proteins: HSPAS, AGTR2, RAGE, and Cathepsin-L.³ For cell lines where data were not available in the Human Protein Atlas server, we conducted a search in the NCBI/GenBank database to determine the taxonomic group to

which the cell line belongs. Subsequently, we performed a protein–protein BLAST search between the potential receptors of the cell line of interest and the receptors expressed in the cell lines present in the Human Protein Atlas, focusing on genomic, proteomic, and functional relationships within the specific tissue/region/cell type.

2.2. Design of Hypothetical Cellular Expression Systems from Experimental Data. We have developed a collection of four hypothetical multiexpression systems to mimic the simultaneous involvement of multiple proteins in four different cell lines: Vero E6, HEK293, HeLa, and CaLu3. These systems incorporate a set of nine proteins, namely, NRP1, CD147, FURIN, TMPRSS2, ACE2, HSPA5, AGTR2, RAGE, and Cathepsin-L (see Table 1).^{2–4} Simulating the expression of

Table 1. Summary of the RNA Expression Levels of the Receptors Studied in Different Cell Lines Analyzed in the Atlas of Human Proteins^a

protein(s)	Vero6	HEK293	HeLa	CaLu3
NRP1	5.8	1.7	3.9	33.8
CD147	72.9	88.7	72.4	85.6
FURIN	9.7	10.3	15.8	8.8
TMPRSS2	11.9	0.01	0.01	0.01
ACE2	1.0	0.1	0.01	0.01
HSPA5	35.2	14.3	30.1	24.0
AGTR2	0.01	0.01	0.01	0.01
AGER	1.7	4.9	0.1	0.2
Cathepsin-L	75.7	37.8	100	100

^aThe generated RNA sequencing results are reported as normalized Transcription Values Per Million (nTPM). Numerical values and a pie chart representation of the expression levels of angiotensin-converting enzyme 2 (ACE2), transmembrane serine 2 (TMPRSS2), basigin2 (CD147), FURIN protease, neuropilin 1 (NRP1), heat shock protein A5 (HSPA5), angiotensin II receptor type 2 (AGTR2), receptor for advanced glycation end products (RAGE) and Cathepsin-L.

all of these proteins simultaneously in each cell line is justified by the fact that it is a plausible occurrence. Single-cell studies have revealed significant variations in protein expression among cells, including instances where certain genes are not expressed individually.³³ Consequently, it is essential to consider heterogeneous coexpression patterns. By simulating these group expression scenarios (systems), we can explore how the susceptibility of cells may be influenced by the type, number, and level of expression of proteins that potentially act as receptors.³³

To assess the susceptibility of cell lines to SARS-CoV-2 infection, we employed the expression levels of potential receptors as a baseline. Utilizing transcriptomics data sourced from The Human Protein Atlas, we classified genes based on their expression patterns in specific tissues, individual cell types, brain regions, blood cells, and cell lines. The RNA expression values were obtained by normalizing the transcription values per million (nTPM) for each gene in tissue culture cell lines. The nTPM value represents the highest expression level found in The Human Protein Atlas transcriptomics database. An nTPM value of ≥ 1 indicates expression in at least one tissue, region, or cell type. Conversely, an nTPM value of < 1 suggests a lack of expression.²⁸

To mitigate potential errors stemming from database limitations and detection methods for expression levels, it has been proposed to assign minimum expression values.¹⁵ Following this recommendation, we considered an nTPM

value of 0.0 to be equivalent to 0.01. This is because values of 0.0 or less may be attributed to data constraints rather than a lack of protein expression. For a comprehensive understanding of transcriptomic data normalization, classification, and data sources, we encourage referring to The Human Protein Atlas' essays and annotations section.³⁰

2.3. Simulation of Viral Dynamics from Experimental Data. To depict our findings, we utilized an in vitro data set of SARS-CoV-2 virus infection in cell lines specifically recommended for culturing the virus. In order to assess the virus's theoretical infectivity based on the susceptibility level mediated by protein expression associated with virus receptors, we held the viral titer constant, with a multiplicity of infection (MOI) set to 1. This approach aligns with previous studies.^{14,34–40} The purpose of this MOI value is to ensure a consistent probability of infection and to consider the recommended viral load necessary for inducing cytopathological effects postinfection (pi).³⁵ In addition, we assumed an initial cell concentration of approximately 1×10^5 cell/mL, which is in line with previous research.^{2,14,15,38} The infection measurement was scheduled at 24 h postinfection (hpi), a time frame consistent with prior investigations.^{14,37,39–41} Notably, earlier reports suggest that several cell lines can reach their maximum infectious SARS-CoV-2 titer in plaque assays within 24 hpi.^{37,42}

To calculate the hypothetical concentration of target or susceptible cells based on the type and level of protein expression, the following steps were undertaken:

1. The same initial total number of cells/mL (approximately 1×10^5) as previously described for each cell line was assumed.
2. Given the low expression levels of certain crucial receptors in specific cell lines, minimum expression values were assigned on a percentage scale. This was done to estimate the hypothetical number of cells and the percentage of expressed receptors, following a suggestion put forth.¹⁵

To determine the effective infection rate (β), a value of 2 was assumed, taking into account the reported basic reproduction number, ρ .¹²

In this sense, each nTPM value was assumed to represent the percentage value of susceptible cells. To do this, we considered the mean of the nTPM values reported for the potential receptors and for each cell line. To address the hypothesis regarding cell susceptibility based on receptor expression levels, a constrained model of target cells was employed. This model relies on available data and aims to estimate infection rates among susceptible cells. Specifically, we utilized a well-established viral infection model known as the limited target cell model.^{15,26} This model encompasses three compartments: susceptible cells (U), infected cells (I), and viral titers (V). The applied model is represented by the following set of differential equations:

$$\frac{dU}{dt} = -\beta UV \quad (1)$$

$$\frac{dI}{dt} = \beta UV - \delta I \quad (2)$$

The equations' left-hand side represents the rate of change of the variables over time. The parameters β and δ denote the effective infection rates and the number of deceased infected cells, respectively. In this model, the virus (V) is assumed to infect susceptible cells (U) at a rate of β , while infected cells are eliminated at a rate of δ . Using this framework, we calculated the

basic reproduction number, R_0 . This value represents the average number of cells that a single infected cell can infect at the beginning of an infection:

$$R_0 = p\beta U / \delta(c + \beta U) \quad (3)$$

Virions are actively released from infected cells at a productive rate of p per day. These virions are either cleared from the circulation at a rate of c or lost upon infecting a target cell. For the virus clearance rate, c , we adopted a value of 10 days^{-1} , as recommended elsewhere.¹⁵ The rate p , which is approximately equal to $22.7 \text{ copies days}^{-1} \text{ cell}^{-1}$, is suggested to be dependent on the susceptible cell population (U). Therefore, to estimate the actual rate p , it is necessary to calculate the product of p and U , as proposed elsewhere.¹⁵

2.4. Drugs with Potential Antiviral Activity Aimed at Blocking the SARS-CoV-2 Receptor-Binding Domain (RBD) Interactions with Host Receptors. In this study, we considered the crystal structure of the RBD complex (PDB: 6MOJ) that facilitates the interaction between SARS-CoV-2 and cellular receptors, such as ACE2. The structure was obtained from the RCSB protein database, as suggested.¹⁹ To gather the pharmacokinetic/pharmacodynamic properties of drugs with reported potential antiviral activity, specifically targeting the SARS-CoV-2 spike protein or viral entry through host receptors, we relied on the literature sources. These sources provided kinetic models and parameter values for drugs like camostat,¹⁶ hydroxychloroquine,¹⁷ nafamostat,¹⁸ ibuprofen,^{19,20} chloroquine,^{17,21} captopril,^{22,23} and telmisartan.²² Additionally, we searched for reported in vitro EC_{50} values, which can be found in Table 2. Likewise, pyronaridine was included as a positive

Table 2. Estimates of the Number of Susceptible Cells (U), Dead Infected Cells (δ), Productive Release Rate of Virions from Cells (p), and Basic Reproduction Number (R_0)

system	U (cell/mL)	p (copies-cell ⁻¹ day ⁻¹)	δ (cell/mL)	R_0
Vero E6	2.4×10^4	5.4×10^5	1.3×10^4	20.5
HEK293	1.8×10^4	4.0×10^5	9.8×10^3	20.3
HeLa	2.5×10^4	5.6×10^5	1.4×10^4	20.6
CaLu3	2.8×10^4	6.4×10^5	1.5×10^4	20.7

control for docking, as it is a ligand tested with AutoDock-based algorithms under similar blind docking conditions to those considered in this study and targeted to the RBD-ACE2 complex. Furthermore, pyronaridine also exhibits thermodynamically favorable binding, as confirmed experimentally by enzyme-linked immunosorbent assay and biolayer interferometry.⁴³

2.5. Prediction of the Affinity and Theoretical Stability of Compounds Targeting the SARS-CoV-2 Receptor-Binding Domain (RBD). Due to the limitations described associated with molecular dockings such as variations in the performance of each method and the inherent limitations of crystal structures to accurately reflect the dynamic nature of protein structures in their biological state, a comparative analysis was performed using various popular molecular docking models to ensure consistent quality for the majority of the targets as suggested.⁴⁴ The complexes were built using the DINC server (<https://dinc.kavrakilab.org/>), which offers a version for the analysis of structures associated with COVID-19 with the docking algorithms AutoDock Vina (Vina), AutoDock Vina RaDii Optimized (Vinardo), and AutoDock 4 (AD4). Addi-

tionally, the DockThor server (<https://www.dockthor.lncc.br/>) was also used, which is a sophisticated machine learning algorithm that utilizes the refined PDBbind data set for training, similar to Vina. These programs were selected due to their advanced and enhanced features, making them improved versions of molecular docking tools. They are based on the efficient AutoDock algorithm, which has been previously recommended.⁴³ To ensure accuracy, a minimum of 10 runs per program were performed, resulting in approximately 1×10^6 evaluations per run. The default parameters were used for the rest of the settings. As part of the preparation, all water molecules were removed, and the PDB files were separated into two distinct files: one containing the protein and the other containing the ligand structure. During the sampling process, only the three runs with the most favorable binding poses were considered. This approach allowed us to focus on the most feasible and thermodynamically favorable positions in the complexes. Based on this criterion, the selected complexes underwent further analysis, including potential theoretical inhibition and molecular dynamics. The binding constant K_i , derived from the binding free energy, was calculated using the equation described:^{19,20}

$$K = e^{-(\Delta G/RT)} \quad (4)$$

And the inhibition constant for binding of ligand to proteins (K_i) (in units of M) was obtained as

$$K_i = K^{-1} = e^{(\Delta G/RT)} \quad (5)$$

In the provided equation, ΔG represents the binding affinity in kcal mol⁻¹, R denotes the universal gas constant ($1.987 \text{ cal K}^{-1} \text{ mol}^{-1}$), and T represents the absolute temperature (298.15 K). According to the equation, a higher K_i value indicates weaker binding between the inhibitor and the protein. Consequently, the protein–inhibitor complex is more likely to dissociate.^{45–47} To determine the IC_{50} values, the Dixon plot was employed, assuming competitive inhibition, as recommended.⁴⁷ This plot offers a reliable estimation of IC_{50} values for competitive inhibition of a specific substrate.⁴⁸ In this study, we considered a hypothetical substrate–inhibitor relationship (1:1) to avoid concentration-driven preferential associations, assuming structural similarities between the ligand and the substrate. Additionally, the IC_{50} -to- K_i web tool was utilized to predict theoretical inhibition potential following the considerations for competitive inhibition with the following equation:

$$IC_{50} = P_{50} = K_i(PL_{50}/[L_{50}]) \quad (6)$$

The variables in the equation include P_{50} , which represents the protein concentration at 50% inhibition; K_i , denoting the affinity constant of the ligand to the protein; $[PL_{50}]$, indicating the protein concentration divided by the ligand concentration at 50% inhibition; and $[L_{50}]$, representing the ligand concentration at 50% inhibition. To predict the concentration of the inhibitor required to achieve 50% inhibition (IC_{50}), we utilized the IC_{50} -to- K_i web tool. This tool utilizes the provided values of $[P]$, $[L]$, and K_i (all units in μM) to generate the IC_{50} value. All calculations were performed using the IC_{50} -to- K_i web tool, accessible at https://bioinfo-abcc.ncifcrf.gov/IC50_Ki_Converter/index.php.^{19,46} On the other hand, the experimental inhibitory concentration values were obtained in molar expression, as described later for each of the compounds considered.^{43,49–60}

Simulations were conducted on docking hits for two main purposes:

1. To examine the relative stability of the ligand within the binding pocket.
2. To sample the minimum energy conformations and assess the perturbation of thermodynamic and structural stability in the complexes.

For each protein–ligand complex, a series of minimization procedures were performed to relax the MD system. This process involved three phases: relaxation, equilibrium, and sampling, as recommended.^{19,61,62} The MD simulation was carried out in an explicit water system. Specifically, the system was solvated in a cubic water box with dimensions of 80 Å for each axis (*X*, *Y*, *Z*). The system consisted of 12424 water molecules, 58 Na⁺ ions, and 34 Cl[−] ions, resulting in a molar density of Na/Cl = 2.76 × 10^{−3}. Each MD system included one copy of the protein system and one copy of the docking ligand. The topology files for the ligands and proteins were automatically generated by using myPresto. The Amber99SB-ILDN force field and the TIP3P water model were employed. The entire system was neutralized, and water molecules were treated as rigid bodies in all models. The simulation time interval was set to 2 fs, and periodic boundary conditions were applied. Temperature and pressure control were achieved using the Berendsen algorithm. After an initial energy minimization phase, which involved steepest descent (5,000 steps) and conjugate gradient (5,000 steps) methods with positional restraints on the solute, a 100 ps simulation was conducted. During this simulation, the positions of the solute atoms were restrained by a force constant of 10 kcal mol^{−1} Å^{−2}. This allowed the water molecules to diffuse around the molecule and to equilibrate the system. The particle mesh Ewald (PME) method was used to calculate the electrostatic contribution to nonbonded interactions with a cutoff distance of 14.0 Å and a time step of 1 fs. The van der Waals interaction cutoff distance was also set to 14.0 Å. Following the equilibration run, a production run was performed at a constant temperature of 300 K using the NVT (particle numbers, volume, and temperature) ensemble. The cell size remained the same, and the SHAKE algorithm was applied to the system. The time step for this run was set to 2 fs. Ten structures were extracted from a 100 ns trajectory, with each structure obtained every 10 ns. These structures served as target structures for further analysis. The root mean square deviation (RMSD) calculations were performed using the following equation:

$$\text{RMSD} = \sqrt{\frac{1}{n} \sum_{i=1}^n \delta_i^2} \quad (7)$$

where δ_i is the distance between atom *i* and either a reference structure or the mean position of the *n* equivalent atoms. The neutralization of this type of system as well as the final production run of 100 ns with a subsequent molecular mechanics/Poisson–Boltzmann surface area (MM/PBSA) calculation has already been widely proposed by other specialists for the study of ligand–protein systems associated with COVID-19. In addition, diverse MD simulation analyses were incorporated including RMSD, RMSF, and R_{gr} as well as comparisons with positive controls as suggested.^{43,64} For the calculation of the root-mean-square fluctuation (RMSF) the algorithm of Calculations and Analysis of Normal Modes WEBnm@ (<http://apps.cbu.uib.no/webnma3/>) was used.⁶³ All MD simulations and additional adjustments were carried out

using COSGENE/myPresto.^{19,61,62} As part of the simulations, binding affinities were predicted based on the force constant relative to the initial frame for each complex during the 100 ns MD simulation. The WebPSN algorithm (accessible at <http://webpsn.hpc.unimo.it/wpsn.php>) was employed to calculate the binding force using two alternative versions of Elastic Network Models (ENM). These models were utilized to evaluate the cross-correlation of the motion of C α atoms and the pairwise interactions between C α atoms. The two versions of ENM used were linear cutoff-ENM and Kovacs-ENM.⁶⁵

To reevaluate the complexes and determine the free energy binding (ΔG_{bind}) of the MD trajectories, we employed the widely used MM/PBSA method^{66–69} as a thermodynamic integration approach. The final snapshots of the minimized system were subjected to MM/PBSA rescoring, which was implemented in AMBER16. As suggested,^{43,64} 2500 frames extracted from the last 10 ns of molecular dynamics were used to compute the solvation free energy and molecular mechanics potential energy for estimation of total binding affinity of the complexes of interest. The formulas for the MM/PBSA binding free energy estimation are shown in eqs 8 and 13:

$$\Delta G_{\text{bind}} = G_{\text{complex}} - (G_{\text{receptor}} + G_{\text{ligand}}) \quad (8)$$

$$= \Delta H - T\Delta S \quad (9)$$

$$\approx \Delta E_{\text{MM}} + \Delta G_{\text{solv}} - T\Delta S \quad (10)$$

$$\Delta E_{\text{MM}} = \Delta E_{\text{bonded}} + \Delta E_{\text{ele}} + \Delta E_{\text{vdw}} \quad (11)$$

$$\Delta G_{\text{solv}} = \Delta G_{\text{polar}} + \Delta G_{\text{nonpolar}} \quad (12)$$

$$\Delta G_{\text{nonpolar}} = \gamma(\Delta \text{SASA}) + \beta \quad (13)$$

The total binding free energy (ΔG_{bind}) represents the difference in free energy between the bound state (G_{complex}) and the free state ($G_{\text{receptor}} + G_{\text{ligand}}$). It can also be expressed as the sum of the enthalpy (ΔH) and entropy part ($-T\Delta S$). In this study, the enthalpy changes were computed using the MM/PBSA approaches, while the entropy changes were neglected due to their computational cost and lower accuracy. The enthalpy part can be further divided into the molecular mechanical energy (ΔE_{MM}) and the solvation free energy (ΔG_{solv}). The ΔE_{MM} term includes the intramolecular energy (ΔE_{bonded}), the electrostatic energy (ΔE_{ele}), and the van der Waals energy (ΔE_{vdw}). The ΔG_{solv} term encompasses both the polar contribution (ΔG_{polar}) and the nonpolar contribution ($\Delta G_{\text{nonpolar}}$). The polar contributions are accounted for using the Poisson–Boltzmann (PB) model, while the nonpolar contributions are assumed to be proportional to the solvent-accessible surface area (SASA).⁷⁰ To calculate the energetic components and predict electrostatic solvation and free binding energies, we utilized the size-modified Poisson–Boltzmann equation (SMPBE) available at <https://web.uwm.edu/smpbs/> and the APBS program accessible at <https://server.poissonboltzmann.org/>.⁶⁶ The ΔG_{bind} of the complexes was determined based on frames extracted after a 100 ns cycle. For visualization and analysis, we employed Molegro Molecular Viewer, version 7.0 (MMV_7.0). Detailed parameters for the MM/PBSA calculation procedures can be found in the Supporting Information Table S1.

2.6. Prediction of Theoretical Antiviral Effectiveness of Ligand from Experimental Data. As mentioned in previous studies,^{15,72,73} we assume that compounds exhibiting antiviral properties with a constant effectiveness ε can reduce R_0 by a

factor of $(1 - \varepsilon)$. In eq 14, ε can take values ranging from 50% to 99%:

$$\varepsilon = \frac{C^n}{K_d^n + C^n} \quad (14)$$

In the equation, C represents the concentration of the ligand in molar units, ε denotes the effect caused by the ligand at concentration C , and K_d stands for the equilibrium dissociation constant. In classical dose–response curves, K_d is referred to as EC_{50} (dose for 50% effect), while in inhibition screens, it is known as IC_{50} (50% inhibition). The Hill coefficient, denoted as n , is a measure of the ligand's response or efficacy ε , which can range from 0 (no drug effect) to 1 (maximum effect). The Hill coefficient can be greater or less than 1, with values of $n < 1$, indicating negative cooperativity, and $n > 1$, indicating positive cooperativity. Typically, small molecules that bind to a target with a single drug-binding site exhibit an uncooperative dose–response curve with a slope parameter of $n = 1$, representing the fraction of bound ligand. For the purposes of this study, we assumed this value.^{15,71} The Hill equation describes the relationship between the fraction of bound ligands and the ligand concentration. The dimension of K_d (IC_{50} or EC_{50}) in this inhibition approximation of the Hill equation is M (molar), as suggested.^{72,73} Additionally, due to limitations in determining the concentrations of active pharmaceutical ingredients (APIs) within the cellular medium of the compounds considered in this study, as they are not approved drugs for the inhibition of SARS-CoV-2, and given the incompatibility in the Hill equations to establish the relationship between the administered drug doses and the API concentrations at the cytoplasmic level, it was theoretically assumed that the reference values for ligand concentration corresponded to the experimental molar inhibitory concentration values reported for each of the compounds,^{43,49–60} in order to illustrate the potential application of the Hill mathematical model. In this regard, the predictions of ε made in this study are only demonstrative, and further studies considering precise API values are recommended. On the other hand, it has been described that antiviral drugs that reduce viral infectivity β by a factor $(1 - \varepsilon_\beta)$ reduce the basic reproductive number, R_0 , by a factor:

$$1 - f(\varepsilon_\beta) = 1 - \frac{c\varepsilon_\beta}{c + (1 - \varepsilon_\beta)\beta U} \quad (15)$$

If $(1 - f(\varepsilon_\beta))R_0$ is less than 1, the virus will almost surely go extinct.⁷⁴ The relationship $(1 - f(\varepsilon_\beta))R_0$ to describe the theoretical antiviral efficacy after treatment was designated in this work with the letter “ ϕ ” for illustrative purposes.

2.7. Prediction of Theoretical Drug Toxicity. Designed to predict potential toxicity, eMolTox is a web server (<http://xundrug.cn/moltox>) that can assess the likely toxic properties of a given molecule. By leveraging advanced machine learning methodologies, eMolTox not only forecasts but also presents comprehensive information about the potential toxic characteristics of a molecule. It also provides comparative data on known toxic compounds, thereby aiding safety analysis in the process of drug development.⁷⁵ Furthermore, the obtained data was cross-referenced with ProTox-II, a server available at https://tox-new.charite.de/prottox_II/index.php?site=home. ProTox-II utilizes molecular similarity, fragment propensities, and machine learning techniques to predict a range of toxicity end points. These end points include acute toxicity, hepatotoxicity, cytotoxicity, carcinogenicity, mutagenicity, immunotoxicity,

adverse outcome pathways, and toxicity targets.⁷⁶ It is important to note that these comparative analyses were conducted despite the fact that most of the compounds considered in this study are FDA-approved, indicating their safety for humans (<https://pubchem.ncbi.nlm.nih.gov/>). Therefore, they far exceed the preclinical judgment provided by computational tools. The purpose of this is to demonstrate their potential toxicity at the cellular level due to limitations in determining the concentrations of the Active Pharmaceutical Ingredients (APIs) within the cellular medium of the compounds considered in this study. This is particularly because they are not FDA-approved drugs for the inhibition of SARS-CoV-2, and it was theoretically assumed that the experimental inhibitory concentration values serve as the theoretical concentrations of the APIs at the cytoplasmic level.

3. RESULTS AND DISCUSSION

3.1. Theoretical Susceptibility to SARS-CoV-2 Infection Depending on the Type and Expression Level of Potential Receptors in Cells of Interest from Experimental Data. A statistically significant difference was observed between the consensus normalized expression levels (nTPM) of proteins associated with SARS-CoV-2 infection in the cell lines studied ($F_{(8, 27)} = 29.524, p < 0.00001, \alpha = 0.01$). No correlation was found between the nTPM levels of any of the proteins studied, regardless of the cell line type. The only exception was a moderate negative correlation between the CD147 protein, and all potential receptors tested ($r \approx -0.50$). A similar correlation was observed between NRP1 and AGTR2, Cathepsin-L, and HSPA5 ($r \approx -0.50$ and $r \approx -0.60$, respectively). As expected, a perfect and positive correlation was observed between the ACE2 receptor and the TMPRSS2 protease ($r = 0.99$). On the other hand, very high and negative correlations were observed between the AGTR2 protein and Cathepsin-L ($r = -0.99$) and between CD147 and HSPA5 ($r = -0.92$). The results of the principal components analysis (PCA) showed that the ACE2 and TMPRSS2 receptors, together with the possible CD147 and HSPA5 receptors, are responsible for most of the observed variability (Cp1 $\approx 46\%$). The positive correlation between the ACE2 receptor and the TMPRSS2 protease as well as its relevance as they are expressed simultaneously has been previously reported.⁷⁷

Under the conditions of this study, all multiple theoretical expression systems were predicted to have a similar susceptibility (U) of up to $\approx 30\%$ cells/mL, with a mean of $\approx 2.4 \times 10^4$ and range of 1.8×10^4 – 2.8×10^4 potentially susceptible cells/mL. Specifically, the CaLu3 system was predicted to have the highest theoretical susceptibility, mediating a susceptibility of $\approx 2.8 \times 10^4$ cells/mL, followed by the Vero E6 and HeLa systems, with a theoretical susceptibility of $\approx 2.4 \times 10^4$ cells/mL. The HEK293 system was the least susceptible to infection under the conditions of this study ($\approx 1.8 \times 10^4$ cells/mL). Although the susceptibility values are very close, the difference in terms of percentage susceptibility between the CaLu3 system and the rest of the systems was between 11 and 37% (see Table 2). These results are consistent with what has been reported because, although all the cell lines tested in this study have shown susceptibility to SARS-CoV-2, it has been reported that SARS-CoV-2 pseudovirions can significantly increase in CaLu3 cells as well as in Vero E6 cells (the cell line most used to replicate and isolate SARS-CoV-2). Meanwhile, HEK293 cells have been characterized as showing modest viral replication.⁷⁸

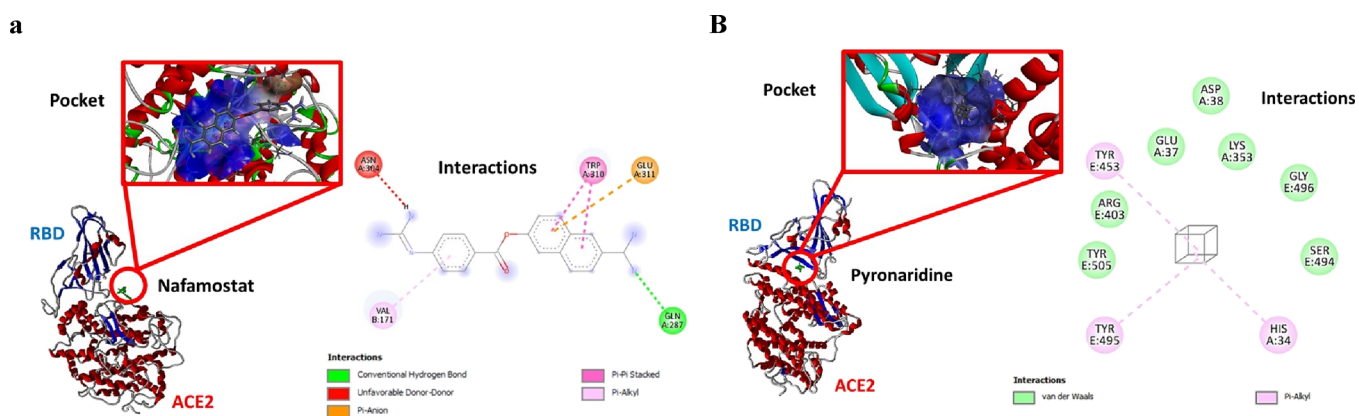


Figure 1. To illustrate, we present the most stable conformation of two compounds: (a) nafamostat (PubChem CID_4413) and (b) pyronaridine (control) (PubChem CID_107771) within the binding pocket of the interface connecting the ACE2 receptor and the receptor-binding domain (RBD). The position and orientation of the nafamostat and pyronaridine structures are indicated within a circle, while the closest residues are displayed in the lower right corner. These interactions were predicted by using the BIOVIA Discovery Studio Visualizer tool. In the context of this study, nafamostat exhibited the most favorable pose within the interface formed between the RBD of SARS-CoV-2 and ACE2.

According to the primary variables considered in this study, the difference in susceptibility is due to the simulated contribution of the possible receptors in each cell line. In the CaLu3 system, CD147 and Cathepsin-L receptors could contribute more than 90% of the observed susceptibility. HeLa and Vero E6 followed, with contributions of more than 80% and 70% of the observed susceptibility by the same potential receptors, respectively. It is important to note that the receptors with the highest correlation in terms of nTPM (ACE2 and TMPRSS2) had a significant contribution in the Vero E6 model ($\approx 6\%$), while in the rest of the cellular models, their average contribution was low ($\approx 0.05\%$). These results allow us to infer that the higher propensity to infection in CaLu3-type systems could also be associated at a statistical level with the contribution of other potential receptors other than ACE2 and TMPRSS2, as has been reported.²

Relative to the number of virions that could theoretically be released from productively infected susceptible cells, the systems tested were predicted to have a mean (p) release rate of 5.3×10^5 copies/cell/day. Specifically, the CaLu3 system was predicted to have the most favorable release rate (p) with a value of 6.4×10^5 copies/cell/day. The least favorable release rate (p) was for HEK293 with 4.0×10^5 copies/cell/day. The theoretical number of dead infected cells (δ) was also predicted, and it was calculated that the tested systems could generate dead cells with a mean of 1.3×10^4 cells/mL. The minimum and maximum values were 9.8×10^3 and 1.5×10^4 cells/mL, respectively, in the HEK293 and CaLu3 cell lines (see Table 2). This behavior in terms of the virions that could be released from infected cells has already been reported.⁷⁸

In order to validate the susceptibility of the cell lines used in this study, the basic reproduction number (R_0) was calculated. R_0 represents the average number of susceptible cells that become infected from a single infected cell at the beginning of the infection. A mean $R_0 \approx 20$ was predicted in all systems. In all cell lines, a $R_0 \geq 20$ was predicted, with a minimum of $R_0 = 20.3$ and a maximum of $R_0 = 20.7$, for the HEK293 and CaLu3 systems, respectively. When comparing the predicted values of R_0 for the group of renal cell lines (Vero E6 and HEK293) against the group of nonrenal cell lines (HeLa and CaLu3), it was found that the difference is not significant ($t = -1.543$, $p = 0.183$, $\alpha = 0.01$) under the conditions of this study, assuming equal variances with a normal distribution of the basic

reproduction number. This suggests that the considered cell lines show similar viral kinetic behavior (see Table 2). The absence of difference between the values of R_0 for the studied cell groups is important because it corresponds to the spectrum of cell lines susceptible to viral infection by coronavirus, which has been reported as similar for the spike protein of SARS-CoV-2, with confirmed entry in CaLu3, HEK293, and Vero E6 cells.⁷⁹

Viruses are considered to infect susceptible cells (U) at an effective infection rate (β) according to eqs 1 and 2 (see section materials and methods). It was assumed that the normalized transcriptional values per million (nTPM) represent the percentage value of U . To do this, the average of the nTPM values reported for potential receptors and each cell line was considered. To calculate the basic reproduction number (R_0), eq 3 was used, where virions are released from infected cells productively at a rate per day (p), generating a number of dead infected cells (δ).

However, under the conditions of this study, the predictions made differ from those of other reports. These reports indicate that virus production tends to be higher in Vero cells than in CaLu3 cells after SARS-CoV-2 infection. These reports suggest that in Vero cells, SARS-CoV-2 entry is mediated by cathepsin L rather than TMPRSS2 due to low or rare expression of TMPRSS2.⁸⁰ However, RNA expression analysis from normalized cell line transcript values reported in The Human Protein Atlas differs from these statements and points to higher TMPRSS2 expression in Vero cells than in CaLu3 cells.²⁸ These discrepancies could affect predictions in terms of cell susceptibility and hence estimates of viral replication.

3.2. Theoretical Affinity of Targeted Drugs for Disruption of SARS-CoV-2 Receptor-Binding Domain (RBD). Table 4 shows the results of the molecular docking methods and scoring functions used to predict the relative binding energies of the considered drugs to the SARS-CoV-2 spike system. All drugs showed thermodynamically favorable binding, with a mean of -8.30 kcal mol⁻¹. Telmisartan showed the most favorable thermodynamic mean, with an energy of ≈ -9.45 kcal mol⁻¹. Followed by the anticoagulant nafamostat (≈ -9.15 kcal mol⁻¹) (see Figure 1). The rest of the analyzed compounds showed a thermodynamically favorable binding energy of ≈ -7 kcal mol⁻¹. In all cases, captopril was the compound with the least favorable binding energy (≈ -5.56 kcal mol⁻¹), very similar to the control drug used (see 3).

Table 3. Comparative Analysis of Various Affinity Parameters of the Drugs and Controls Considered in This Study against the Receptor-Binding Domain (RBD) of SARS-CoV-2

drug ^a	types	kcal mol ⁻¹				K _i (μ M) ^d	Binding force ^e (kcal.mol ⁻¹ Å ⁻²)	MM/PBSA ^e (kcal.mol ⁻¹)	Interface RBD ^g
		DockT ^b	Vina ^c	Vinardo ^c	AD4 ^c				
telmisartan (CID_65999)	ARBs	-8.71	-9.65	-9.70	-9.72	0.13	8.96	-4.03	-
nafamostat (CID_4413)	anticoagulant	-7.47	-9.75	-9.94	-9.45	0.23	9.18	-10.38	+
camostat (CID_2536)	serine protease inhibitor	-7.38	-8.18	-8.00	-7.72	1.99	9.31	-15.24	-
hydroxychloroquine (CID_3652)	antimalarials	-7.97	-6.84	-7.84	-7.84	2.79	9.78	-8.72	-
chloroquine (CID_2719)	antimalarials	-7.76	-7.04	-7.77	-7.77	2.98	9.20	-13.79	-
ibuprofen (CID_3672)	NSAID	-7.24	-7.35	-7.93	-6.65	4.85	9.34	-9.75	-
captopril (CID_44093)	ARBs	-6.40	-5.95	-4.77	-5.13	88.55	9.26	-7.61	-
pyronaridine (CID_107771) (control)	antimalarials	-7.60	-5.31	-5.09	-4.22	0.36 ^{f*}	7.78	-3.27	+

^aAll compounds were obtained from the PubChem database (<https://pubchem.ncbi.nlm.nih.gov/>). ^bScore calculated from DockThor (<https://dockthor.lncc.br/v2/>). ^cScore calculated from DINC (<http://dinc.kavrakilab.org/>). ^dTheoretical inhibitory kinetics of each ligand-protein complex calculated from the mean energy. ^eForce constant and Molecular Mechanics/Poisson–Boltzmann surface area (MM/PBSA) calculations from the minimum energy structures of the complexes after an MD of 100 ns. ARBs, angiotensin II receptor blockers; NSAID, nonsteroidal anti-inflammatory drugs. ^fExperimental values (see section materials and methods). ^gThe negative sign (-) is used to designate the docking outside the interface established by the RBD with receptors like ACE2, and the positive sign (+) to indicate the docking that occurs within the interface.

Table 4. Results of the Predicted Kinetics and Inhibitory Potency of the Drugs Considered in This Study in Terms of IC₅₀ and pIC₅₀ on the SARS-CoV-2 Receptor-Binding Domain (RBD)

drug ^a	EC ₅₀ (M) ^b	pEC ₅₀ ^b	IC ₅₀ (M) ^c	pIC ₅₀ ^c	IC ₅₀ (M) ^d	pIC ₅₀ ^d
telmisartan (CID_65999)	1.0 × 10 ⁻⁷	5.0	1.9 × 10 ⁻⁸	7.7	6.9 × 10 ⁻⁸	7.2
nafamostat (CID_4413)	1.0 × 10 ⁻⁷	7.0	3.5 × 10 ⁻⁸	7.5	1.0 × 10 ⁻⁷	7.0
camostat (CID_2536)	1.0 × 10 ⁻⁶	6.0	3.0 × 10 ⁻⁷	6.5	3.1 × 10 ⁻⁷	6.5
hydroxychloroquine (CID_3652)	4.2 × 10 ⁻⁶	5.4	4.2 × 10 ⁻⁷	6.4	3.4 × 10 ⁻⁷	6.5
chloroquine (CID_2719)	4.4 × 10 ⁻⁶	5.4	4.5 × 10 ⁻⁷	6.3	3.5 × 10 ⁻⁷	6.5
ibuprofen (CID_3672)	2.5 × 10 ⁻⁵	4.6	7.3 × 10 ⁻⁷	6.1	3.9 × 10 ⁻⁷	6.4
captopril (CID_44093)	1.0 × 10 ⁻⁵	5.0	1.3 × 10 ⁻⁵	4.9	4.9 × 10 ⁻⁷	6.3
pyronaridine (CID_107771) (control)			4.5 × 10 ^{-5e}	4.3 ^e	1.0 × 10 ^{-8d}	8.0 ^d

^aAll compounds were obtained from the PubChem database (<https://pubchem.ncbi.nlm.nih.gov/>). ^bValues calculated in molar expression from the experimental data (see section materials and methods). ^cValues calculated in molar expression from theoretical binding kinetics and relative energies using the Dixon plot method. ^dValues calculated in molar expression from theoretical binding kinetics and relative energies using the IC50-to-K_i web tool (https://bioinfo-abcc.ncifcrf.gov/IC50_Ki_Converter/index.php). EC₅₀, half maximal effective concentration; pEC₅₀, negative logarithm of the EC₅₀ value; IC₅₀, concentration at which the drug is capable of inhibiting activity by 50%; pIC₅₀, negative logarithm of the IC₅₀ value ^eExperimental values (see section materials and methods).

These results correspond to reports that compounds such as nafamostat and camostat have very favorable binding energy values against the coronavirus spike glycoprotein. Indeed, nafamostat has shown the most favorable interactions and inhibitory power in previous experiments.⁸¹ Moreover, the results garnered with Vinardo carry a significant weight. This is because Vinardo is an algorithm that boasts superior docking, scoring, classification, and virtual evaluation capabilities, consistently outperforming both Vina and AD4. It can classify active compounds over inactive ones. Vinardo (Vina RaDii Optimized) is a scoring function that incorporates component terms similar to those of the Vina scoring function. These component terms include steric interactions, hydrophobic interactions, and nondirectional hydrogen bonds. However, Vinardo distinguishes itself from Vina through several modifications. It features a modified steric interaction term, utilizes new atomic radii, and employs simplified interactions.⁸²

In terms of the theoretical inhibitory kinetics of each ligand–protein complex, which was calculated from the respective relative energies of binding, a mean K_i = 14.50 μ M was predicted, with a minimum and maximum inhibition constant for the compounds telmisartan (K_i = 0.13 μ M) and captopril (K_i

= 88.55 μ M), respectively. Approximately 70% (5/7) of the tested compounds (targets of this study) showed a theoretical inhibition constant K_i < 3 μ M. Only a value close to 28% (2/7) of the compounds had a K_i < 0.5 μ M (telmisartan and nafamostat), similar to what was described for the control drug (K_i \approx 0.4 μ M) (see Table 4). Additionally, binding affinities based on the relative force constant and free energy binding calculation (ΔG_{bind}) considering the MM/PBSA method on the final lowest energy structures after MD predicted thermodynamically favorable docking. In the case of the force constant calculation, a mean of \approx 9 kcal mol⁻¹ Å⁻² was predicted, with a minimum and maximum of 8.96 and 9.78 kcal mol⁻¹ Å⁻² for the compounds telmisartan and hydroxychloroquine, respectively. While with MM/PBSA, a mean of \approx -9 kcal mol⁻¹ was predicted, with a minimum and maximum of \approx -15 kcal mol⁻¹ Å⁻² and \approx -4 kcal mol⁻¹ for the camostat and telmisartan compounds, respectively (see Table 3).

As the relevance of the ACE2 receptor in mediating infection has been confirmed, its interaction with the SARS-CoV-2 receptor-binding domain (RBD) was studied.⁸³ The interface formed between the RBD and ACE2 was explored for illustrative purposes only. Of the compounds tested and under the

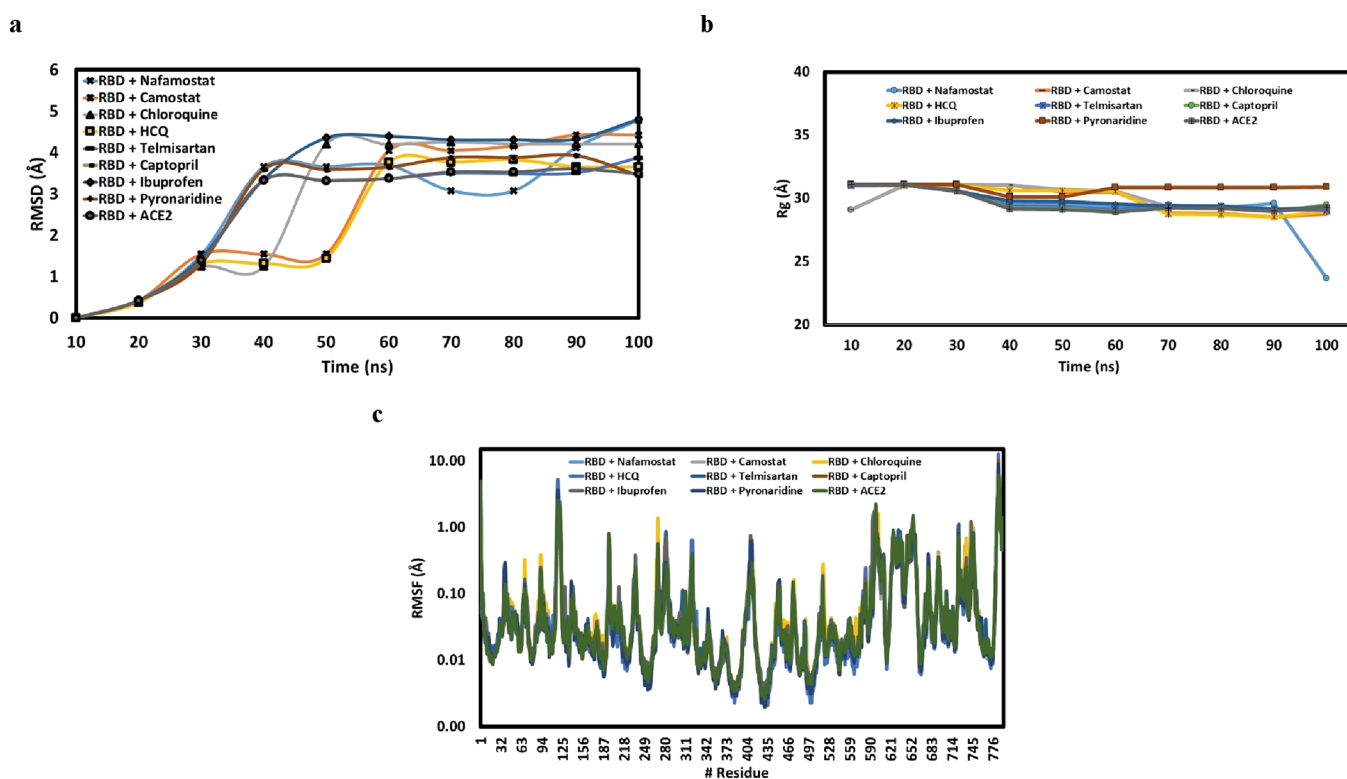


Figure 2. MD simulation for each complex (total time 100 ns). (a) Root mean squared deviations (RMSD) of C α during each 10 ns, (b) root means square fluctuation (RMSF), and (c) radius of gyration-guided motions (R_g). RBD, receptor-binding domain; HCQ, hydroxychloroquine.

conditions of this study, only nafamostat showed favorable poses in the interface formed between the receptor-binding domain (RBD) of SARS-CoV-2 and ACE2 after 24 runs with a total of 10^6 evaluations per run, similar to what was described for the pyronaridine control (see Figures 1–3 and Table 3). The poses presented by nafamostat turned out to be the most statistically likely to be among the top three thermodynamically most favored scores out of a total of 2.4×10^7 possible positions, which were guided by blind docking. In all cases, the interactions of the compounds with the spike were dominated by hydrophobic interactions, with the greatest diversity of types of interactions observed for the compound camostat. All compounds mediated interactions with a relative binding strength of ≈ 9 kcal mol $^{-1}$ Å $^{-2}$.

In relation to the inhibitory potency calculated from the reported experimental EC $_{50}$ values, a mean potency was predicted in terms of pEC $_{50} = 5.5$. Specifically, nafamostat was predicted to be the compound with the highest theoretical inhibitory potency calculated from the reported experimental EC $_{50}$ values, with a value of pEC $_{50} = 7.0$. While ibuprofen was the compound with the lowest inhibitory potency calculated from the data reported for NSAIDs, with a pEC $_{50} = 4.6$ (see Table 4).

Additionally, the predictions based on EC $_{50}$ were validated applying the Dixon method and the IC $_{50}$ -to- K_i web tool using the theoretical values of IC $_{50}$. In all cases, the inhibitory potency calculated in terms of pIC $_{50}$ was reproducible regardless of the compound and predictive method used (Dixon plot and IC $_{50}$ -to- K_i web tool) for the calculation of IC $_{50}$, showing an overall difference between methods with a mean of ≈ 0.1 , and a difference between the mean of pEC $_{50}$ (experimental data reported) and pIC $_{50} \approx 1$ (see Table 4).

Studies have shown that nafamostat exhibits strong inhibitory effects on coronavirus-mediated membrane fusion in HEK293

and CaLu3 cells.¹⁸ Compared to other compounds such as camostat, nafamostat has demonstrated more favorable inhibitory activity. This superiority has been attributed to nafamostat's ability to readily form a stable covalent enzyme–substrate intermediate, which effectively explains its high potency. These findings align with in vitro experiments and are consistent with previous virus cell entry assays.⁸⁴

Molecular dynamics simulations showed that upon ligand binding, all complexes exhibited conformational fluctuations with an RMSD of ≤ 3.2 Å. These results in terms of RMSD indicate that the junctions are stable throughout the simulation period of 100 ns. This is in addition to being thermodynamically favorable (as previously predicted). These observations together with the predictions in terms of RMSF and R_g allow us to infer that all the tested compounds form stable complexes (see Figure 2). It is important to note that both nafamostat and the pyronaridine control were compound-guided by blind docking and showed interactions with the RBD interface that were predicted to be stable over time according to the molecular dynamics (MD) simulation analysis at 100 ns and in terms of RMSD, RMSF, R_g , and the number and type of interactions (see Figure 3). Despite these standard theoretical approaches showing promising favorable and stable interactions over time for the complexes considered in this study, it is recommended to validate the predictions of such systems through lead compound similarity analysis in order to better understand the behavior of each selected drug against the target protein, as suggested.^{85,86}

3.3. Prediction of Theoretical Antiviral Effectiveness of Drugs from Experimental Data. Table 5 shows the prediction of the theoretical antiviral effectiveness of each of the compounds considered based on the susceptibility of the cell type. Predictions made from reported experimental EC $_{50}$ (μ M) and IC $_{50}$ (μ M) values calculated in this study from relative

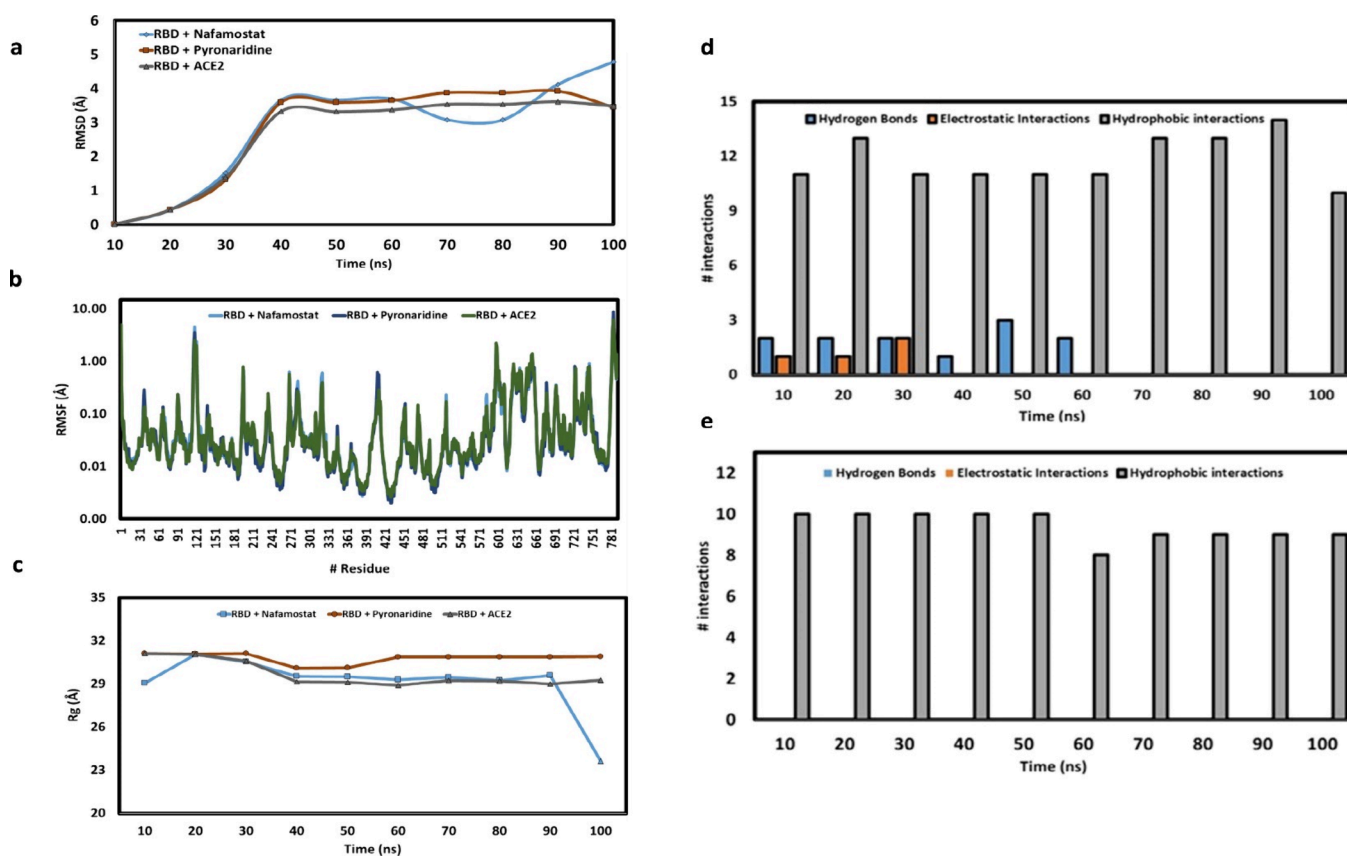


Figure 3. MD simulation of compounds with the most favorable pose in the interface formed between the RBD of SARS-CoV-2 and cellular receptors like ACE2 under the conditions of this study (total time of 100 ns). (a) Root mean squared deviations (RMSDs) of $C\alpha$ during each 10 ns, (b) root means square fluctuation (RMSF), (c) radius of gyration-guided motions (R_g), (d) number and type of interactions of nafamostat, and (e) pyronaridine. RBD, receptor-binding domain.

binding energies and theoretical inhibitory kinetics are presented. In terms of antiviral effectiveness calculated from the EC_{50} , similar mean drug efficacy was predicted as a function of cell type susceptibility ($F_{(3,24)} = 0.002$, $p = 0.999$, $\alpha = 0.01$) with an effect in percentage terms of $\approx 68\%$.

However, a statistically significant difference was predicted between the individual antiviral effectiveness of each of the compounds tested ($F_{(6,21)} = 4088.756$, $p < 0.00001$, $\alpha = 0.01$). From the EC_{50} values, it was predicted that $\approx 42\%$ (3/7) of the considered drugs may show a theoretical antiviral effectiveness $\geq 80\%$. Specifically, the compound nafamostat was predicted to have the highest theoretical antiviral effectiveness, regardless of the type of simulated cell susceptibility, with $\approx 99\%$ effectiveness, followed by camostat ($\approx 86\%$) and chloroquine ($\approx 80\%$).

While ibuprofen presented the lowest predicted theoretical antiviral effectiveness ($\approx 28\%$). In the HEK293 cell line, the theoretical antiviral effect of approximately 42% (3/7) of the tested compounds (telmisartan, captopril, and ibuprofen) was slightly less favorable followed by a similar behavior in the Vero E6 and HeLa lines. On the other hand, and in a strict (but not significant) sense, the lowest theoretical antiviral response was predicted in the CaLu3 system under the conditions of this study.

For illustrative purposes, we sought to predict and compare the theoretical antiviral effectiveness of the compounds from the IC_{50} values calculated in this study. The predictions with the Dixon plot model reproduced the trend calculated from the EC_{50} values (although with a greater magnitude of the values) showing a similar mean response of the cells ($F_{(3,24)} = 0.020$, $p =$

0.996 , $\alpha = 0.01$) and also a statistically significant difference between the antiviral effectiveness of each of the compounds tested ($F_{(6,21)} = 196.708$, $p < 0.00001$, $\alpha = 0.01$). It is important to note that, just like the values of binding free energy (ΔG) and K_p , the values in terms of IC_{50} and pIC_{50} presented by the control are also within the predicted values for each compound considered in this study. Therefore, a similar behavior would be expected in terms of theoretical antiviral activity (see Table 4).

It is important to point out that after applying the Dixon method and the IC_{50} -to- K_i web tool to estimate the IC_{50} values, an increase in the theoretical antiviral effectiveness of all of the compounds was observed. This decreased the discriminatory capacity of the model proposed here by using the EC_{50} experimental values. However, regardless of the method applied to calculate the IC_{50} , nafamostat presented the highest theoretical antiviral effectiveness in each case (see Table 5). It is important to note that one of the limitations of this study is that the predictions of antiviral efficacy, made from the kinetic/dynamic properties reported for the drugs studied, only consider a single initial dose of each drug for 24 h. This is consistent with the findings of previous studies of other drugs, such as hydroxychloroquine,¹⁷ nafamostat,^{51,52} camostat,⁵³ telmisartan,⁵⁴ chloroquine,⁵⁵ ibuprofen,⁵⁶ and captopril.^{57,58} With this in mind, we suggest conducting an analysis under the same conditions as this study but with variations in concentration taken into account as well as extending the exposure time to the drugs under investigation. This approach has been recommended in other studies.¹⁵

Table 5. Results of the Predicted Antiviral Efficacy (ϵ) of the Drugs Considered in This Study from the EC_{50} and IC_{50} Values and in Relation to the Types of Cell Lines Studied

drug(s) ^a	EC_{50} (μM) ^b	antiviral efficacy (%) ^e			
		Vero E6	HeLa	HEK293	CaLu3
nafamostat	0.1	99	99	99	99
camostat	1	86	86	86	86
chloroquine	4.4	80	80	80	80
hydroxychloroquine	4.2	72	72	72	72
telmisartan	10	57	57	59	56
captopril	10	57	57	59	56
ibuprofen	25	28	28	29	28

drug(s) ^a	IC_{50} (μM) ^c	antiviral efficacy (%)			
		Vero E6	HeLa	HEK293	CaLu3
nafamostat	0.03	99	99	99	99
camostat	0.3	95	95	95	95
chloroquine	0.45	97	97	97	97
hydroxychloroquine	0.42	97	97	97	97
telmisartan	0.02	99	99	99	99
captopril	13.28	89	89	91	88
ibuprofen	0.73	94	94	94	94

drug(s) ^a	IC_{50} (μM) ^d	antiviral efficacy (%)			
		Vero E6	HeLa	HEK293	CaLu3
nafamostat	0.1	99	99	99	99
camostat	0.31	95	95	95	95
chloroquine	0.35	98	98	98	98
hydroxychloroquine	0.34	97	97	97	97
telmisartan	0.07	98	98	98	98
captopril	0.49	88	88	88	88
ibuprofen	0.39	97	97	97	97

^aAll compounds were obtained from the PubChem database (<https://pubchem.ncbi.nlm.nih.gov/>). ^bValues calculated in molar expression from the experimental data (see section materials and methods). ^cValues calculated in molar expression from theoretical binding kinetics and relative energies using the Dixon plot method. ^dValues calculated in molar expression from theoretical binding kinetics and relative energies using the IC_{50} -to- K_i web tool (https://bioinfo-abcc.ncifcrf.gov/IC50_Ki_Converter/index.php). EC_{50} , half maximal effective concentration; pEC_{50} , negative logarithm of the EC_{50} value; IC_{50} , concentration at which the drug is capable of inhibiting activity by 50%; pIC_{50} , negative logarithm of the IC_{50} value. ^ePercentage expression of the reduction in viral infectivity (ϵ) in terms of the effective radius of infection (β) by the factor $(1 - \epsilon_\beta)$.

The findings of this study regarding the antiviral activity and the impact of drugs on the viral kinetics of SARS-CoV-2 have previously been reported in cell lines such as CaLu3 and HEK293 with other coronaviruses. Nafamostat has been shown to possess superior antiviral activity compared to camostat against MERS-CoV.^{17,18} Conversely, the camostat has demonstrated activity against the TMPRSS2 receptor, partially inhibiting spike-driven entry into Caco-2, Vero E6, and CaLu3 cells against MERS-CoV, SARS-CoV-1, and SARS-CoV-2. However, it has been suggested that the spread of SARS-CoV-2 relies on the activity of multiple receptors, which could explain the partial inhibition of viral activity in CaLu3 cells when exposed to camostat.^{16,17}

While chloroquine and hydroxychloroquine are currently used for the treatment of malaria and amebiasis, studies have reported their potential to block the interaction between the SARS-CoV spike protein's receptor-binding domain (RBD) and ACE2 under cell culture conditions in Vero E6 cells. Both

chloroquine and hydroxychloroquine have the ability to increase the endosomal pH, which is necessary for the conformational changes in the spike protein during virus-cell fusion. Additionally, these compounds can affect the terminal glycosylation of the cellular receptor ACE2, thereby reducing the affinity of SARS-CoV/SARS-CoV-2 for ACE2.^{17,21}

Although there is affinity in energetic terms, a generalized effect of inhibitory activity of captopril and telmisartan was not observed. This could be because these compounds have more affinity for the ACE2 cell receptor than for viral spike regions without compromising the activity of ACE2. This has been reported previously.^{22,23} Although the predicted results with ibuprofen correspond to a potential ability to interact favorably with the spike protein, as has been reported,^{19,20,59} no significant inhibitory activity was observed under the conditions of this study. Ibuprofen has been extensively studied in cell lines, including CaLu3. It has been shown that this drug has no effect on ACE2 modulation, despite hypotheses earlier in the pandemic. This has led to the conclusion that there are no risks associated with the use of nonsteroidal anti-inflammatory drugs (NSAIDs) like ibuprofen during a SARS-CoV-2 infection.⁵⁹

The theoretical susceptibility previously predicted for each of the cell lines considered was used as a control of the tests to evaluate the theoretical antiviral activity of the drugs (Table 2 and Figure 3). For illustrative purposes, the effect of drugs on the number of susceptible cells and the effect of their potential antiviral activity on the number of cells to be infected were simulated. Specifically, antiviral drugs that reduce viral infectivity in terms of the effective radius of infection (β) by the factor $(1 - \epsilon_\beta)$ reduce the basic reproductive number, R_0 , by a factor $(1 - f(\epsilon_\beta))$. If $(1 - f(\epsilon_\beta))R_0$ is <1 , the virus will almost certainly become extinct.

In this sense, the relationship $(1 - f(\epsilon_\beta))R_0$ to describe the theoretical antiviral efficacy of drugs after *in vitro* treatment for 24 h was designated as ϕ . In all the cell lines tested, a mean of the relationship $\phi \approx 0.065$ was predicted, indicating that in all the cell models considered, a decrease in total viral particles is predicted. This effect was simulated for a period of 24 h exposure to drugs, with the HEK293 system being the cell line where the greatest inhibition effect was predicted, but without a statistically significant difference ($F_{(3,24)} = 0.003$, $p = 0.999$, $\alpha = 0.01$) (see Table 6).

In relation to the individual activity of the drugs, it was predicted that under the conditions of this study, all the compounds could theoretically have the capacity to reduce viral infectivity by different magnitudes in terms of the effective radius of infection (β) and reduce the basic reproductive number, R_0 , (ϕ ratio) in all cell lines tested. Specifically, in relation to the individual drug activity, nafamostat was predicted to be the compound with the highest ability to reduce β -viral infectivity and to reduce the R_0 number ($\phi = 0.002$) in all considered cell lines. It was followed by camostat ($\phi = 0.029$) and chloroquine ($\phi = 0.041$), with ibuprofen being the least favorable compound ($\phi = 0.147$) (Table 6).

Given that renal and pulmonary cell systems were simulated, it is important to note that all the compounds considered in this study are widely known drugs approved by the FDA with known kinetic and dynamic characteristics (all compounds were obtained from the PubChem database: <https://pubchem.ncbi.nlm.nih.gov/>). Therefore, the prediction of potential toxicities was also carried out using the latest generation of machine learning analysis applied to experimental data *in vitro* and *in vivo*

Table 6. Predicted Antiviral Efficacy of the Drugs Considered in This Study in Terms of the ϕ Relationship Calculated from the Reduction in the Effective Radius of Infection (β) and the Reduction in the Basic Reproductive Number, R_0 with Respect to the Cell Lines Studied

drug(s) ^a	antiviral efficacy ($\phi = (1 - f(\varepsilon_\beta))R_0$) ^b			
	Vero E6	HeLa	HEK293	CaLu3
nafamostat	0.002	0.002	0.002	0.002
camostat	0.029	0.028	0.029	0.029
chloroquine	0.041	0.041	0.041	0.041
hydroxychloroquine	0.057	0.057	0.058	0.058
telmisartan	0.088	0.087	0.084	0.091
captopril	0.088	0.087	0.084	0.091
ibuprofen	0.148	0.146	0.146	0.149

^aAll compounds were obtained from the PubChem database (<https://pubchem.ncbi.nlm.nih.gov/>). ^bThe relationship $(1 - f(\varepsilon_\beta))R_0$ designated in this study as ϕ describes the theoretical antiviral efficacy of drugs after in vitro treatment for 24 h. Antiviral drugs that reduce viral infectivity in terms of the effective radius of infection (β) by the factor $(1 - \varepsilon_\beta)$ reduce the basic reproductive number, R_0 , by a factor $(1 - f(\varepsilon_\beta))$. If $\phi = (1 - f(\varepsilon_\beta))R_0$ is <1 , the virus will almost certainly become extinct (see section materials and methods).

and related to toxicology and the analysis of the toxic substructure. Around 77% (7/9) of the tested compounds may be potentially toxic in at least one type of organ or tissue, with a statistical significance of more than 99%. Specifically, $\approx 55\%$ (5/9) of the compounds may be potentially toxic at the renal level, while $\approx 22\%$ (2/9) may be potentially toxic at the respiratory level. It is important to note that only nafamostat and camostat did not demonstrate any toxic action from data-driven models (https://tox-new.charite.de/prottox_II/index.php?site=home). These predictions hold significance due to the utilization of the eMolTox method (<http://xundrug.cn/moltox>), which incorporates a comprehensive set of 174 in vitro/in vivo experimental data sets pertaining to toxicology for model development (Supporting Information Tables S2–S8). The method further employs Mondrian's conformal prediction (MCPs) to estimate the confidence level associated with the generated predictions.⁷⁵

As shown in Figures 4 and 5, the most favorable drugs such as nafamostat and camostat mediated a theoretical decrease in the number of infected cells (I) and the number of dead infected cells (δ) despite the mock susceptibility (U). The theoretical activity presented by compounds like nafamostat can be attributed to the impact of the reduction in the effective radius of infection (β) by the factor $(1 - \varepsilon_\beta)$, which in turn translates into a reduction in the basic reproductive number, R_0 , by a factor $(1 - f(\varepsilon_\beta))$. Specifically, the effective infection ratio was calculated as $\beta \approx 0.31$, which represents an overall theoretical reduction of the simulated daily rate of infection by $\approx 15\%$ with respect to reported values used as control ($\beta = 2$).¹² Consistently, nafamostat was the compound predicted to reduce the daily effective infection rate the most ($\beta = 0.01$) in all simulated cell models (see Figure 4B, Supporting Information Figures S1–S6). Followed by camostat in HEK293 ($\beta = 0.14$) (see Figure 5B) and chloroquine in CaLu3 ($\beta = 0.20$), with ibuprofen being the compound with the least effect on viral kinetics (see Supporting Information Figures S1–S6). These predictions based on theoretical models of cell lines correspond with the reports of the usefulness of nafamostat administered for the prevention of SARS-CoV-2 infection, above camostat.⁶⁰

The predictions made in this study indicate that at a theoretical level, it is likely that the infection of cell lines such as CaLu3 may be slightly more favored than in Vero E6 if it is mediated by the contribution of receptors other than ACE2 with a higher level of expression. In a previous work,⁷⁸ in which a smaller number of potential receptors was considered, and without studying the antiviral activity of drugs, our predictions also found that the ACE2 receptor probably does not contribute by itself to explain the theoretical mechanism of infection in CaLu3. However, the limitations reported when measuring the active replication of the virus at a significant level in diverse samples associated with the respiratory tract⁸⁷ do not correspond to the hypothesis of an exclusive participation of potential receptors that exhibit a high level of expression in cells such as CaLu3. This could suggest the involvement of other ACE2-independent cooperative or coupled effects that may mediate theoretical CaLu3 infection, as has been suggested.^{88,89}

On the other hand, the differential behavior of drugs with possible antiviral properties against SARS-CoV-2 was observed

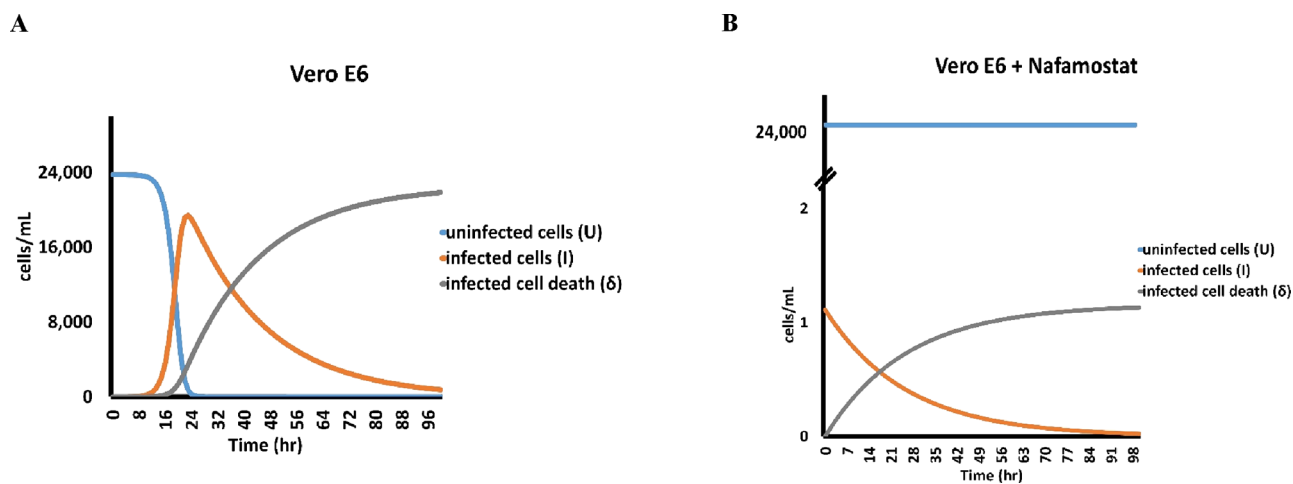


Figure 4. Mechanistic model is employed to estimate the rates of uninfected cells (U), infected cells (I), and death of infected cells (δ). For illustrative purposes, a representative graph of the expression systems mentioned in the text is provided for each cell line studied using the limited target cell model. Additional graphics can be found in Supporting Information Figures S1–S6. (A) Vero E6 cell line and (B) Vero E6 + nafamostat.

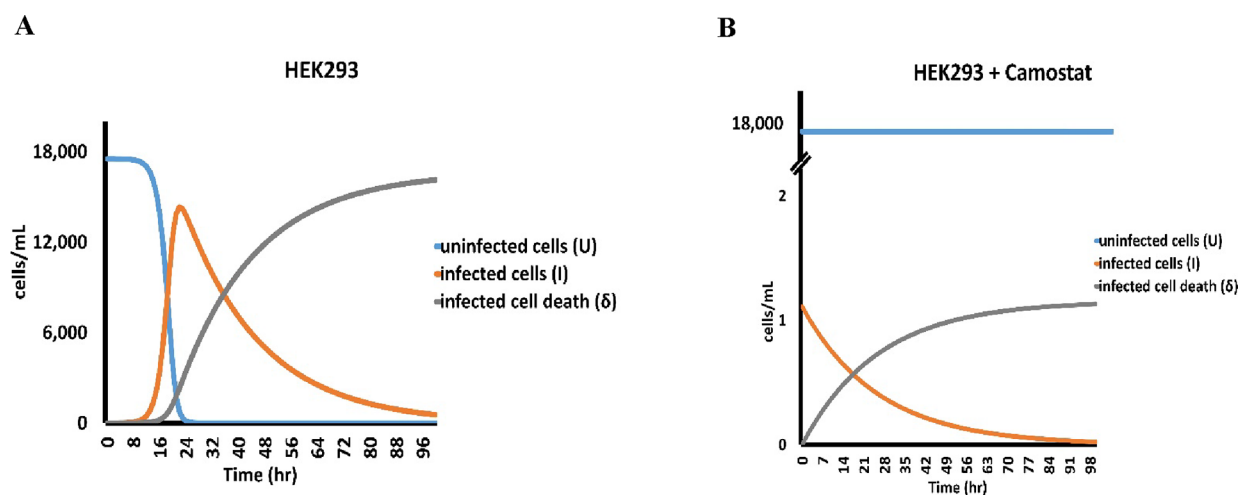


Figure 5. Mechanistic model is utilized to provide estimates of the rates of uninfected cells (U), infected cells (I), and death of infected cells (δ). To enhance our understanding, a representative graph depicting the expression systems mentioned in the text is included for each cell line studied using the limited target cell model. Supporting Information Figures S1–S6 contain additional graphics. (A) HEK293 cell line, (B) HEK293 + camostat, (C) CaLu3 cell line, and (D) CaLu3 + nafamostat.

depending on the type of simulated cell line, as has been reported.⁵⁰ In fact, it has been pointed out that CaLu3 cells tend to be more sensitive to inhibitors than HEK293 cells, even with the use of compounds such as nafamostat and camostat.¹⁸ As an instance, camostat, which functions as an inhibitor of the plasma membrane protease TMPRSS2, has exhibited activity in CaLu3 cells while not displaying the same effect in Vero E6 cells, as anticipated in this study. This reinforces the significance of comprehending the translatability of a cellular model of infection,⁸⁰ especially as camostat has been reported to have no antiviral effects *in vivo* in animal models compared to nafamostat.⁶⁰

Indeed, studies of this nature are crucial, as they provide theoretical backing for the impact of the intricate multiple entry mechanisms associated with SARS-CoV-2. This underscores the necessity to select optimal cell lines for compound evaluation and screening, particularly in studies aimed at uncovering broad antiviral mechanisms.⁸⁵ Finally, it is important to point out that these cell line-based predictions contribute to the tracing of possible routes of infection, the prediction of potentially susceptible organs, and the investigation of interventions for the prevention, control, and treatment of infection by theoretically proposing ideal cell models. These are relevant aspects considering that it has been found that cell lines grown under standard laboratory conditions have difficulties in reproducing the behavior of cells that live in patients.⁹¹

4. CONCLUSIONS

Theoretical cellular systems considered and simulated, which express multiple receptors simultaneously, have demonstrated susceptibility similar to SARS-CoV-2. Additionally, the anticipated viral kinetic behavior in the simulated cell lines aligns with the conditions of this study. Among the cell lines tested, the CaLu3 system is projected to be the most susceptible to SARS-CoV-2 infection. This susceptibility can be attributed statistically to the presence of receptors such as CD147 and Cathepsin-L, which likely contribute significantly to the observed susceptibility. Nafamostat, among the compounds tested, exhibits the most favorable characteristics in terms of thermodynamics, kinetics, theoretical antiviral activity, and potential safety (toxicity) associated with SARS-CoV-2 spike

protein-mediated infections in the tested cell lines. This study provides mathematical and bioinformatic models for identifying optimal cell lines for evaluating and detecting compounds, particularly in studies focused on the antiviral mechanisms of drugs for potential reuse. It is important to note that these observations must be experimentally validated, and this research is expected to stimulate future quantitative experiments.

■ ASSOCIATED CONTENT

Supporting Information

The Supporting Information is available free of charge at <https://pubs.acs.org/doi/10.1021/acsomega.3c06968>.

Mechanistic model of the estimates of the rates of uninfected cells (U), infected cells (I), and death of infected cells (δ) (Figures S1–S6); detailed parameters for the MM/PBSA calculation procedures (Table S1) (PDF)

Supporting information on compound toxicity (Tables S2–S8) (XLS)

■ AUTHOR INFORMATION

Corresponding Author

Lenin González-Paz – Centro de Biomedicina Molecular (CBM). Laboratorio de Biocomputación (LB), Instituto Venezolano de Investigaciones Científicas (IVIC), Maracaibo, Zulia 4001, República Bolivariana de Venezuela; orcid.org/0000-0003-0023-7342; Email: lgonzalezpaz@gmail.com

Authors

Carla Lossada – Centro de Biomedicina Molecular (CBM). Laboratorio de Biocomputación (LB), Instituto Venezolano de Investigaciones Científicas (IVIC), Maracaibo, Zulia 4001, República Bolivariana de Venezuela

María Laura Hurtado-León – Facultad Experimental de Ciencias (FEC). Departamento de Biología. Laboratorio de Genética y Biología Molecular (LGBM), Universidad del Zulia (LUZ), Maracaibo 4001, República Bolivariana de Venezuela

Juan Vera-Villalobos – Facultad de Ciencias Naturales y Ambientales, Departamento de Química y Ciencias Ambientales, Laboratorio de Análisis Químico Instrumental

(LAQUINS), Escuela Superior Politécnica del Litoral, Guayaquil EC090112, Ecuador

José L. Paz – Departamento Académico de Química Inorgánica, Facultad de Química e Ingeniería Química, Universidad Nacional Mayor de San Marcos, Lima 15081, Perú; orcid.org/0000-0002-6177-7919

Yovani Marrero-Ponce – Grupo de Medicina Molecular y Traslacional (MeM&T), Colegio de Ciencias de la Salud (COCSA), Escuela de Medicina, Edificio de Especialidades Médicas; e Instituto de Simulación Computacional (ISC-USFQ), Diego de Robles y vía Interoceánica, Universidad San Francisco de Quito (USFQ), Quito, Pichincha 170157, Ecuador

Felix Martinez-Rios – Universidad Panamericana. Facultad de Ingeniería, Ciudad de México 03920, México

Ysaías J. Alvarado – Centro de Biomedicina Molecular (CBM). Laboratorio de Química Biofísica Teórica y Experimental (LQBTE), Instituto Venezolano de Investigaciones Científicas (IVIC), Maracaibo, Zulia 4001, República Bolivariana de Venezuela; orcid.org/0000-0002-2709-409X

Complete contact information is available at:

<https://pubs.acs.org/10.1021/acsomega.3c06968>

Author Contributions

L.G.P.: Conceptualization, Methodology, Investigation, Writing – Reviewing and Editing. C.L. and M.L.H.-L.: Investigation. J.V.-V.: Reviewing. J.L.P.: Writing – Reviewing, Original draft preparation. Y.M.-P.: Writing – Reviewing, Original Draft Preparation. F.M.-R.: Reviewing. Y.J.A.: Writing – Reviewing and Editing, Conceptualization.

Funding

This research did not receive any specific grant from funding agencies in the public, commercial, or not-for-profit sector.

Notes

The authors declare no competing financial interest.

ACKNOWLEDGMENTS

This research was supported by regular funds of the Venezuelan Institute for Scientific Research (IVIC). J.L.P. thanks the Vicerrectorado de Investigación y Postgrado of the Universidad Nacional Mayor de San Marcos for the computational resources used.

REFERENCES

- (1) Chen, Y.; Liu, Q.; Guo, D. Emerging coronaviruses: Genome structure, replication, and pathogenesis. *J. Med. Virol.* **2020**, *92* (4), 418–423.
- (2) Fenizia, C.; Galbiati, S.; Vanetti, C.; Vago, R.; Clerici, M.; Tacchetti, C.; Daniele, T. SARS-CoV-2 Entry: At the Crossroads of CD147 and ACE2. *Cell* **2021**, *10* (6), 1434.
- (3) Kyrou, I.; Randevara, H. S.; Spandidos, D. A.; Karteris, E. Not only ACE2—the quest for additional host cell mediators of SARS-CoV-2 infection: Neuropilin-1 (NRP1) as a novel SARS-CoV-2 host cell entry mediator implicated in COVID-19. *Signal transduction and targeted therapy* **2021**, *6* (1), 1–3.
- (4) Dobrindt, K.; Hoagland, D. A.; Seah, C.; Kassim, B.; O'Shea, C. P.; Murphy, A.; Iskhakova, M.; Fernando, M. B.; Powell, S. K.; Deans, P. J. M.; Javidfar, B.; Peter, C.; Moller, R.; Uhl, S. A.; Garcia, M. F.; Kimura, M.; Iwasawa, K.; Crary, J. F.; Kotton, D. N.; Takebe, T.; Huckins, L. M.; tenOever, B. R.; Akbarian, S.; Brennard, K. J. Common genetic variation in humans impacts in vitro susceptibility to SARS-CoV-2 infection. *Stem Cell Rep.* **2021**, *16* (3), 505–518.
- (5) Jafary, F.; Jafari, S.; Ganjalikhany, M. R. In silico investigation of critical binding pattern in SARS-CoV-2 spike protein with angiotensin-converting enzyme 2. *Sci. Rep.* **2021**, *11* (1), 1–13.
- (6) Hikmet, F.; Méar, L.; Edvinsson, Å.; Micke, P.; Uhlén, M.; Lindskog, C. The protein expression profile of ACE2 in human tissues. *Molecular systems biology* **2020**, *16* (7), No. e9610.
- (7) Campbell, R. A.; Boilard, E.; Rondina, M. T. Is there a role for the ACE2 receptor in SARS-CoV-2 interactions with platelets? *Journal of Thrombosis and Haemostasis* **2021**, *19* (1), 46–50.
- (8) Whittaker, G. R. SARS-CoV-2 spike and its adaptable FURIN cleavage site. *Lancet Microbe* **2021**, *2* (10), e488–e489.
- (9) Johnson, B. A.; Xie, X.; Bailey, A. L.; et al. Loss of FURIN cleavage site attenuates SARS-CoV-2 pathogenesis. *Nature* **2021**, *591*, 293–299.
- (10) Bollavaram, K.; Leeman, T. H.; Lee, M. W.; Kulkarni, A.; Upshaw, S. G.; Yang, J.; Song, H.; Platt, M. O. Multiple sites on SARS-CoV-2 spike protein are susceptible to proteolysis by cathepsins B, K, L, S, and V. *Protein science: a publication of the Protein Society* **2021**, *30* (6), 1131–1143.
- (11) Keyaerts, E.; Vijgen, L.; Maes, P.; Neyts, J.; Ranst, M. V. Growth kinetics of SARS-coronavirus in Vero E6 cells. *Biochem. Biophys. Res. Commun.* **2005**, *329* (3), 1147–1151.
- (12) Bar-On, Y. M.; Flamholz, A.; Phillips, R.; Milo, R. Science Forum: SARS-CoV-2 (COVID-19) by the numbers. *Elife* **2020**, *9*, No. e57309.
- (13) Liu, F.; Han, K.; Blair, R.; Kenst, K.; Qin, Z.; Upcin, B.; Wörsdörfer, P.; Midkiff, C. C.; Mudd, J.; Belyaeva, E.; Milligan, N. S.; Rorison, T. D.; Wagner, N.; Bodem, J.; Dölken, L.; Aktas, B. H.; Vander Heide, R. S.; Yin, X. M.; Kolls, J. K.; Roy, C. J.; Rappaport, J.; Ergün, S.; Qin, X. SARS-CoV-2 Infects Endothelial Cells In Vivo and In Vitro. *Frontiers in cellular and infection microbiology* **2021**, *11*, No. 701278.
- (14) Dinesh Kumar, N.; Ter Ellen, B. M.; Bouma, E. M.; Troost, B.; van de Pol, D.; van der Ende-Metselaar, H. H.; van Gosliga, D.; Apperloo, L.; Carpaij, O. A.; van den Berge, M.; Nawijn, M. C.; Stienstra, Y.; Rodenhuis-Zybert, I. A.; Smit, J. M. Moxidectin and Ivermectin Inhibit SARS-CoV-2 Replication in Vero E6 Cells but Not in Human Primary Bronchial Epithelial Cells. *Antimicrob. Agents Chemother.* **2022**, *66* (1), No. e0154321.
- (15) Gonçalves, A.; Bertrand, J.; Ke, R.; Comets, E.; de Lamballerie, X.; Malvy, D.; Pizzorno, A.; Terrier, O.; Rosa Calatrava, M.; Mentré, F.; Smith, P.; Perelson, A. S.; Guedj, J. Timing of antiviral treatment initiation is critical to reduce SARS-CoV-2 viral load. *CPT: Pharmacometrics Syst. Pharmacol.* **2020**, *9* (9), 509–514.
- (16) Hoffmann, M.; Kleine-Weber, H.; Schroeder, S.; Krüger, N.; Herrler, T.; Erichsen, S.; Schiergens, T. S.; Herrler, G.; Wu, N. H.; Nitsche, A.; Müller, M. A.; Drosten, C.; Pöhlmann, S. SARS-CoV-2 cell entry depends on ACE2 and TMPRSS2 and is blocked by a clinically proven protease inhibitor. *Cell* **2020**, *181* (2), 271–280.
- (17) Xiu, S.; Dick, A.; Ju, H.; Mirzaie, S.; Abdi, F.; Cocklin, S.; Zhan, P.; Liu, X. Inhibitors of SARS-CoV-2 entry: current and future opportunities. *Journal of medicinal chemistry* **2020**, *63* (21), 12256–12274.
- (18) Yamamoto, M.; Matsuyama, S.; Li, X.; Takeda, M.; Kawaguchi, Y.; Inoue, J. I.; Matsuda, Z. Identification of nafamostat as a potent inhibitor of Middle East respiratory syndrome coronavirus S protein-mediated membrane fusion using the split-protein-based cell-cell fusion assay. *Antimicrob. Agents Chemother.* **2016**, *60* (11), 6532–6539.
- (19) González-Paz, L. A.; Lossada, C. A.; Fernández-Materán, F. V.; Paz, J. L.; Vera-Villalobos, J.; Alvarado, Y. J. Can Non-steroidal Anti-inflammatory Drugs Affect the Interaction Between Receptor Binding Domain of SARS-COV-2 Spike and the Human ACE2 Receptor? A Computational Biophysical Study. *Front. Phys.* **2020**, *8*, No. 587606.
- (20) Terrier, O.; Dilly, S.; Pizzorno, A.; Chalupska, D.; Humpolickova, J.; Bouřa, E.; Berenbaum, F.; Quideau, S.; Lina, B.; Fève, B.; Adnet, F.; Sabbah, M.; Rosa-Calatrava, M.; Maréchal, V.; Henri, J.; Slama-Schwok, A. Antiviral Properties of the NSAID Drug Naproxen Targeting the Nucleoprotein of SARS-CoV-2 Coronavirus. *Molecules (Basel, Switzerland)* **2021**, *26* (9), 2593.
- (21) Vincent, M. J.; Bergeron, E.; Benjannet, S.; Erickson, B. R.; Rollin, P. E.; Ksiazek, T. G.; Seidah, N. G.; Nichol, S. T. Chloroquine is

a potent inhibitor of SARS coronavirus infection and spread. *Virology journal* **2005**, *2*, 69.

(22) Wysocki, J.; Lores, E.; Ye, M.; Soler, M. J.; Batlle, D. Kidney and lung ACE2 expression after an ACE inhibitor or an Ang II receptor blocker: implications for COVID-19. *Journal of the American Society of Nephrology* **2020**, *31* (9), 1941–1943.

(23) Isaac-Lam, M. F. Molecular modeling of the interaction of ligands with ACE2–SARS-CoV-2 spike protein complex. *In silico pharmacology* **2021**, *9* (1), 1–16.

(24) Nguyen, V. K.; Binder, S. C.; Boianelli, A.; Meyer-Hermann, M.; Hernandez-Vargas, E. A. Ebola virus infection modeling and identifiability problems. *Frontiers in microbiology* **2015**, *6*, 257.

(25) Baccam, P.; Beauchemin, C.; Macken, C. A.; Hayden, F. G.; Perelson, A. S. Kinetics of influenza A virus infection in humans. *Journal of virology* **2006**, *80* (15), 7590–7599.

(26) Nguyen, V. K.; Hernandez-Vargas, E. A. Parameter Estimation in Mathematical Models of Viral Infections Using R. *Methods in molecular biology* **2018**, *1836*, 531–549.

(27) Abernathy, Z.; Abernathy, K.; Stevens, J. A mathematical model for tumor growth and treatment using virotherapy. *AIMS Math* **2020**, *5*, 4136–50.

(28) Digre, A.; Lindskog, C. The human protein atlas—spatial localization of the human proteome in health and disease. *Protein Sci.* **2021**, *30* (1), 218–233.

(29) Zamorano Cuervo, N.; Grandvaux, N. ACE2: Evidence of role as entry receptor for SARS-CoV-2 and implications in comorbidities. *Elife* **2020**, *9*, No. e61390.

(30) Bairoch, A. The cellosaurus, a cell-line knowledge resource. *Journal of biomolecular techniques: JBT* **2018**, *29* (2), 25.

(31) Shilts, J.; Crozier, T. W.; Greenwood, E. J.; Lehner, P. J.; Wright, G. J. No evidence for basigin/CD147 as a direct SARS-CoV-2 spike binding receptor. *Sci. Rep.* **2021**, *11* (1), 1–10.

(32) Chu, H.; Chan, J. F.; Yuen, T. T.; Shuai, H.; Yuan, S.; Wang, Y.; Hu, B.; Yip, C. C.; Tsang, J. O.; Huang, X.; Chai, Y.; Yang, D.; Hou, Y.; Chik, K. K.; Zhang, X.; Fung, A. Y.; Tsoi, H. W.; Cai, J. P.; Chan, W. M.; Ip, J. D.; Chu, A.; Zhou, J.; Lung, D. C.; Kok, K.; To, K.; Tsang, O.; Chan, K. H.; Yuen, K. Y. Comparative tropism, replication kinetics, and cell damage profiling of SARS-CoV-2 and SARS-CoV with implications for clinical manifestations, transmissibility, and laboratory studies of COVID-19: an observational study. *Lancet. Microbe* **2020**, *1* (1), e14–e23.

(33) Peixoto, A.; Monteiro, M.; Rocha, B.; Veiga-Fernandes, H. Quantification of multiple gene expression in individual cells. *Genome research* **2004**, *14* (10a), 1938–1947.

(34) Matsuyama, S.; Kawase, M.; Nao, N.; Shirato, K.; Ujiike, M.; Kamitani, W.; Shimajima, M.; Fukushi, S. The Inhaled Steroid Ciclesonide Blocks SARS-CoV-2 RNA Replication by Targeting the Viral Replication-Transcription Complex in Cultured Cells. *Journal of virology* **2020**, *95* (1), e01648–20.

(35) Modrof, J.; Kerschbaum, A.; Farcet, M. R.; Niemeyer, D.; Corman, V. M.; Kreil, T. R. SARS-CoV-2 and the safety margins of cell-based biological medicinal products. *Biologicals* **2020**, *68*, 122–124.

(36) Schroeder, S.; Pott, F.; Niemeyer, D.; Veith, T.; Richter, A.; Muth, D.; Goffinet, C.; Muller, M. A.; Drosten, C. Interferon antagonism by SARS-CoV-2: a functional study using reverse genetics. *Lancet Microbe* **2021**, *2* (5), e210–e218.

(37) Appelberg, S.; Gupta, S.; Svensson Akusjärvi, S.; Ambikan, A. T.; Mikaeloff, F.; Saccon, E.; Végvári, A.; Benfeitas, R.; Sperk, M.; Ståhlberg, M.; Krishnan, S.; Singh, K.; Penninger, J. M.; Mirazimi, A.; Neogi, U. Dysregulation in Akt/mTOR/HIF-1 signaling identified by proteo-transcriptomics of SARS-CoV-2 infected cells. *Emerging microbes & infections* **2020**, *9* (1), 1748–1760.

(38) Ter Ellen, B. M.; Dinesh Kumar, N.; Bouma, E. M.; Troost, B.; van de Pol, D.; van der Ende-Metselaar, H. H.; Apperloo, L.; van Gosliga, D.; van den Berge, M.; Nawijn, M. C.; van der Voort, P.; Moser, J.; Rodenhuis-Zybert, I. A.; Smit, J. M. Resveratrol and Pterostilbene Inhibit SARS-CoV-2 Replication in Air-Liquid Interface Cultured Human Primary Bronchial Epithelial Cells. *Viruses* **2021**, *13* (7), 1335.

(39) Kishimoto, M.; Uemura, K.; Sanaki, T.; Sato, A.; Hall, W. W.; Kariwa, H.; Orba, Y.; Sawa, H.; Sasaki, M. TMPRSS11D and TMPRSS13 Activate the SARS-CoV-2 Spike Protein. *Viruses* **2021**, *13* (3), 384.

(40) Pontelli, M. C.; Castro, I. A.; Martins, R. B.; Veras, F. P.; Serra, L.; Nascimento, D. C.; Cardoso, R. S.; Rosales, R.; Lima, T. M.; Souza, J. P.; Caetité, D. B.; de Lima, M.; Kawahisa, J. T.; Giannini, M. C.; Bonjorno, L. P.; Lopes, M.; Batah, S. S.; Siyuan, L.; Assad, R. L.; Almeida, S.; Oliveira, F.; Benatti, M.; Pontes, L.; Santana, R.; Vilar, F.; Martins, M.; Cunha, T.; Calado, R.; Alves-Filho, J.; Zamboni, D.; Fabro, A.; Louzada-Junior, P.; Oliveira, R.; Cunha, F.; Arruda, E. Infection of human lymphomononuclear cells by SARS-CoV-2. *bioRxiv: the preprint server for biology* **2020**, DOI: 10.1101/2020.07.28.225912.

(41) Fiege, J. K.; Thiede, J. M.; Nanda, H. A.; Matchett, W. E.; Moore, P. J.; Montanari, N. R.; Thielen, B. K.; Daniel, J.; Stanley, E.; Hunter, R. C.; Menachery, V. D.; Shen, S. S.; Bold, T. D.; Langlois, R. A.; Subbarao, K. Single cell resolution of SARS-CoV-2 tropism, antiviral responses, and susceptibility to therapies in primary human airway epithelium. *PLoS Pathogens* **2021**, *17* (1), No. e1009292.

(42) Zhang, B. Z.; Chu, H.; Han, S.; Shuai, H.; Deng, J.; Hu, Y. F.; Gong, H. R.; Lee, A. C.; Zou, Z.; Yau, T.; Wu, W.; Hung, I. F.; Chan, J. F.; Yuen, K. Y.; Huang, J. D. SARS-CoV-2 infects human neural progenitor cells and brain organoids. *Cell research* **2020**, *30* (10), 928–931.

(43) Coghi, P.; Yang, L. J.; Ng, J. P. L.; Haynes, R. K.; Memo, M.; Gianoncelli, A.; Wong, V. K. W.; Ribaud, G. A drug repurposing approach for antimalarials interfering with SARS-CoV-2 spike protein receptor binding domain (RBD) and human angiotensin-converting enzyme 2 (ACE2). *Pharmaceuticals* **2021**, *14* (10), 954.

(44) Choi, S.; Son, S. H.; Kim, M. Y.; Na, I.; Uversky, V. N.; Kim, C. G. Improved prediction of protein-protein interactions by a modified strategy using three conventional docking software in combination. *Int. J. Biol. Macromol.* **2023**, *252*, No. 126526.

(45) Shamsi, A.; Mohammad, T.; Anwar, S.; AlAjmi, M. F.; Hussain, A.; Rehman, M. T.; Islam, A.; Hassan, M. Glecaprevir and Maraviroc are high-affinity inhibitors of SARS-CoV-2 main protease: possible implication in COVID-19 therapy. *Bioscience Reports* **2020**, *40* (6), BSR20201256.

(46) Cer, R. Z.; Mudunuri, U.; Stephens, R.; Lebeda, F. J. IC50-to-Ki: a web-based tool for converting IC50 to Ki values for inhibitors of enzyme activity and ligand binding. *Nucleic Acids Res.* **2009**, *37* (2), W441–W445.

(47) Li, Z.; Li, X.; Huang, Y. Y.; Wu, Y.; Liu, R.; Zhou, L.; Lin, Y.; Wu, D.; Zhang, L.; Liu, H.; Xu, X.; Yu, K.; Zhang, Y.; Cui, J.; Zhan, C. G.; Wang, X.; Luo, H. B. Identify potent SARS-CoV-2 main protease inhibitors via accelerated free energy perturbation-based virtual screening of existing drugs. *Proc. Natl. Acad. Sci. U. S. A.* **2020**, *117* (44), 27381–27387.

(48) Burlingham, B. T.; Widlanski, T. S. An intuitive look at the relationship of Ki and IC50: a more general use for the Dixon plot. *J. Chem. Educ.* **2003**, *80* (2), 214.

(49) Gutiérrez-Chamorro, L.; Riveira-Muñoz, E.; Barrios, C.; Palau, V.; Nevot, M.; Pedreño-López, S.; Senserrich, J.; Massanella, M.; Clotet, B.; Cabrera, C.; Mitjà, O.; Crespo, M.; Pascual, J.; Riera, M.; Ballana, E. SARS-CoV-2 Infection Modulates ACE2 Function and Subsequent Inflammatory Responses in Swabs and Plasma of COVID-19 Patients. *Viruses* **2021**, *13* (9), 1715.

(50) Reus, P.; Schneider, A. K.; Ulshöfer, T.; Henke, M.; Bojkova, D.; Cinatl, J.; Ciesek, S.; Geisslinger, G.; Laux, V.; Grättinger, M.; Gribbon, P.; Schiffmann, S. Characterization of ACE Inhibitors and AT1R Antagonists with Regard to Their Effect on ACE2 Expression and Infection with SARS-CoV-2 Using a Caco-2 Cell Model. *Life (Basel, Switzerland)* **2021**, *11* (8), 810.

(51) Moon, K.; Hong, K. W.; Bae, I. G. Treatment effect of nafamostat mesylate in patients with COVID-19 pneumonia: study protocol for a randomized controlled trial. *Trials* **2021**, *22* (1), 1–9.

(52) Zhuravel, S. V.; Khmelnytskyi, O. K.; Burlaka, O. O.; Gritsan, A. I.; Goloshchekin, B. M.; Kim, S.; Hong, K. Y. Nafamostat in hospitalized

patients with moderate to severe COVID-19 pneumonia: a randomised Phase II clinical trial. *EclinicalMedicine* **2021**, *41*, No. 101169.

(53) Kitagawa, J.; Arai, H.; Iida, H.; Mukai, J.; Furukawa, K.; Ohtsu, S.; Nakade, S.; Hikima, T.; Haranaka, M.; Uemura, N. A phase I study of high dose camostat mesylate in healthy adults provides a rationale to repurpose the TMPRSS2 inhibitor for the treatment of COVID-19. *Clinical and translational science* **2021**, *14* (5), 1967–1976.

(54) Rothlin, R. P.; Vetulli, H. M.; Duarte, M.; Pelorosso, F. G. Telmisartan as tentative angiotensin receptor blocker therapeutic for COVID-19. *Drug Dev. Res.* **2020**, *81* (7), 768–770.

(55) Gendrot, M.; Javelle, E.; Clerc, A.; Savini, H.; Pradines, B. Chloroquine as a prophylactic agent against COVID-19? *International journal of antimicrobial agents* **2020**, *55* (6), No. 105980.

(56) Smart, L.; Fawkes, N.; Goggin, P.; Pennick, G.; Rainsford, K. D.; Charlesworth, B.; Shah, N. A narrative review of the potential pharmacological influence and safety of ibuprofen on coronavirus disease 19 (COVID-19), ACE2, and the immune system: a dichotomy of expectation and reality. *Inflammopharmacology* **2020**, *28* (5), 1141–1152.

(57) Viveiros, A.; Gheblawi, M.; Aujla, P. K.; Sosnowski, D. K.; Seubert, J. M.; Kassiri, Z.; Oudit, G. Y. Sex-and age-specific regulation of ACE2: Insights into severe COVID-19 susceptibility. *Journal of molecular and cellular cardiology* **2022**, *164*, 13–16.

(58) Kim, G. H. J.; Melgoza, A.; Jiang, F.; Guo, S. The effect of renin–angiotensin–aldosterone system inhibitors on organ-specific ace2 expression in zebrafish and its implications for COVID-19. *Sci. Rep.* **2021**, *11* (1), 1–9.

(59) de Bruin, N.; Schneider, A. K.; Reus, P.; Talmon, S.; Ciesek, S.; Bojkova, D.; Cinatl, J.; Lodhi, L.; Charlesworth, B.; Sinclair, S.; Pennick, G.; Laughy, W. F.; Gribbon, P.; Kannt, A.; Schiffmann, S. Ibuprofen, Flurbiprofen, Etoricoxib or Paracetamol Do Not Influence ACE2 Expression and Activity In Vitro or in Mice and Do Not Exacerbate In-Vitro SARS-CoV-2 Infection. *Int. J. Mol. Sci.* **2022**, *23* (3), 1049.

(60) Owen, A.; Neary, M.; Box, H.; Sharp, J.; Tatham, L.; Curley, P.; Herriott, J. Evaluation of intranasal nafamostat or camostat for SARS-CoV-2 chemoprophylaxis in Syrian golden hamsters. *bioRxiv* **2021**, 2021 DOI: [10.1101/2021.07.08.451654](https://doi.org/10.1101/2021.07.08.451654).

(61) Kasahara, K.; Terazawa, H.; Itaya, H.; Goto, S.; Nakamura, H.; Takahashi, T.; Higo, J. myPresto/omegagene 2020: a molecular dynamics simulation engine for virtual-system coupled sampling. *Biophysics and Physicobiology* **2020**, *17*, 140–146.

(62) González-Paz, L. A.; Lossada, C. A.; Moncayo, L. S.; Romero, F.; Paz, J. L.; Vera-Villalobos, J.; Pérez, A. E.; Portillo, E.; San-Blas, E.; Alvarado, Y. J. A Bioinformatics Study of Structural Perturbation of 3CL-Protease and the HR2-Domain of SARS-CoV-2 Induced by Synergistic Interaction with Ivermectins. *Biointerface Research in Applied. Chemistry* **2021**, *11* (2), 9813 DOI: [10.33263/BRIAC112.98139826](https://doi.org/10.33263/BRIAC112.98139826).

(63) Tiwari, S. P.; Fuglebakk, E.; Hollup, S. M.; Skjærven, L.; Cragnolini, T.; Grindhaug, S. H.; Tekle, K. M.; Reuter, N. WEBnm@v2.0: Web server and services for comparing protein flexibility. *BMC Bioinformatics* **2014**, *15*, 427.

(64) Kumari, R.; Kumar, V.; Dhankhar, P.; Dalal, V. Promising antivirals for PLpro of SARS-CoV-2 using virtual screening, molecular docking, dynamics, and MMPBSA. *J. Biomol. Struct. Dyn.* **2023**, *41* (10), 4650–4666.

(65) Felling, A.; Seeber, M.; Fanelli, F. webPSN v2. 0: a webserver to infer fingerprints of structural communication in biomacromolecules. *Nucleic Acids Res.* **2020**, *48* (W1), W94–W103.

(66) Xie, Y.; Ying, J.; Xie, D. SMPBS: Web server for computing biomolecular electrostatics using finite element solvers of size modified Poisson-Boltzmann equation. *J. Comput. Chem.* **2017**, *38* (8), 541–552.

(67) Sen Gupta, P. S.; Biswal, S.; Panda, S. K.; Ray, A. K.; Rana, M. K. Binding mechanism and structural insights into the identified protein target of COVID-19 and importin- α with in-vitro effective drug ivermectin. *J. Biomol. Struct. Dyn.* **2020**, 1–10.

(68) Mosquera-Yuqui, F.; Lopez-Guerra, N.; Moncayo-Palacio, E. A. Targeting the 3CLpro and RdRp of SARS-CoV-2 with phytochemicals

from medicinal plants of the Andean Region: molecular docking and molecular dynamics simulations. *J. Biomol. Struct. Dyn.* **2020**, 1–14.

(69) Kalhor, H.; Sadeghi, S.; Abolhasani, H.; Kalhor, R.; Rahimi, H. Repurposing of the approved small molecule drugs in order to inhibit SARS-CoV-2 S protein and human ACE2 interaction through virtual screening approaches. *J. Biomol. Struct. Dyn.* **2020**, 1–16.

(70) Wang, Z.; Wang, X.; Li, Y.; Lei, T.; Wang, E.; Li, D.; Kang, Y.; Zhu, F.; Hou, T. farPPI: a webserver for accurate prediction of protein-ligand binding structures for small-molecule PPI inhibitors by MM/PB(GB)SA methods. *Bioinformatics (Oxford, England)* **2019**, *35* (10), 1777–1779.

(71) Perelson, A. S.; Deeks, S. G. Drug effectiveness explained: the mathematics of antiviral agents for HIV. *Science translational medicine* **2011**, *3* (91), 91ps30–91ps30.

(72) Prinz, H. Hill coefficients, dose–response curves and allosteric mechanisms. *Journal of chemical biology* **2010**, *3*, 37–44.

(73) Gesztelyi, R.; Zsuga, J.; Kemeny-Beke, A.; Varga, B.; Juhasz, B.; Tosaki, A. The Hill equation and the origin of quantitative pharmacology. *Archive for history of exact sciences* **2012**, *66*, 427–438.

(74) Czuppon, P.; Débarre, F.; Gonçalves, A.; Tenailon, O.; Perelson, A. S.; Guedj, J.; Blanquart, F. Success of prophylactic antiviral therapy for SARS-CoV-2: Predicted critical efficacies and impact of different drug-specific mechanisms of action. *PLoS computational biology* **2021**, *17* (3), No. e1008752.

(75) Ji, C.; Svensson, F.; Zoufir, A.; Bender, A. eMolTox: prediction of molecular toxicity with confidence. *Bioinformatics (Oxford, England)* **2018**, *34* (14), 2508–2509.

(76) Banerjee, P.; Eckert, A. O.; Schrey, A. K.; Preissner, R. ProTox-II: a webserver for the prediction of toxicity of chemicals. *Nucleic acids research* **2018**, *46* (W1), W257–W263.

(77) González-Paz, L.; Alvarado, M. J.; Hurtado-León, M. L.; Lossada, C.; Vera-Villalobos, J.; Loroño, M.; Paz, J. L.; Jeffreys, L. N.; Torres, F. J.; Alvarado, Y. J. Comparative study of SARS-CoV-2 infection in different cell types: Biophysical-computational approach to the role of potential receptors. *Computers in biology and medicine* **2022**, *142*, No. 105245. Advance online publication.

(78) Takayama, K. In vitro and animal models for SARS-CoV-2 research. *Trends in pharmacological sciences* **2020**, *41* (8), 513–517.

(79) Murgolo, N.; Therien, A. G.; Howell, B.; Klein, D.; Koepflinger, K.; Lieberman, L. A.; Adam, G. C.; Flynn, J.; McKenna, P.; Swaminathan, G.; Hazuda, D. J.; Olsen, D. B. SARS-CoV-2 tropism, entry, replication, and propagation: Considerations for drug discovery and development. *PLoS pathogens* **2021**, *17* (2), No. e1009225.

(80) Park, B. K.; Kim, D.; Park, S.; Maharjan, S.; Kim, J.; Choi, J. K.; Akauliya, M.; Lee, Y.; Kwon, H. J. Differential Signaling and Virus Production in Calu-3 Cells and Vero Cells upon SARS-CoV-2 Infection. *Biomolecules & therapeutics* **2021**, *29* (3), 273–281.

(81) Duru, C. E.; Umar, H. I. U.; Duru, I. A.; Enenebeaku, U. E.; Ngozi-Olehi, L. C.; Enyoh, C. E. Blocking the interactions between human ACE2 and coronavirus spike glycoprotein by selected drugs: a computational perspective. *Environ. Anal. Health Toxicol.* **2021**, *36* (2), No. e2021010, DOI: [10.5620/eaht.2021010](https://doi.org/10.5620/eaht.2021010).

(82) Quiroga, R.; Villarreal, M. A. Vinardo: A scoring function based on autodock vina improves scoring, docking, and virtual screening. *PloS one* **2016**, *11* (5), No. e0155183.

(83) Liu, M.; Wang, T.; Zhou, Y.; Zhao, Y.; Zhang, Y.; Li, J. Potential role of ACE2 in coronavirus disease 2019 (COVID-19) prevention and management. *Journal of translational internal medicine* **2020**, *8* (1), 9–19.

(84) Hempel, T.; Raich, L.; Olsson, S.; Azouz, N. P.; Klingler, A. M.; Hoffmann, M.; Pohlmann, S.; Rothenberg, M. E.; Noé, F. Molecular mechanism of inhibiting the SARS-CoV-2 cell entry facilitator TMPRSS2 with camostat and nafamostat. *Chemical Science* **2021**, *12* (3), 983–992.

(85) Saraswat, J.; Singh, P.; Patel, R. A computational approach for the screening of potential antiviral compounds against SARS-CoV-2 protease: Ionic liquid vs herbal and natural compounds. *Journal of molecular liquids* **2021**, *326*, No. 115298.

(86) Saraswat, J.; Riaz, U.; Patel, R. In-silico study for the screening and preparation of ionic liquid-AVDs conjugate to combat COVID-19 surge. *J. Mol. Liq.* **2022**, *359*, No. 119277.

(87) Sulaiman, I.; Chung, M.; Angel, L.; Tsay, J. C. J.; Wu, B. G.; Yeung, S. T.; Krolikowski, K.; Li, Y.; Duerr, R.; Schluger, R.; Thannickal, S. A.; Koide, A.; Rafeq, S.; Barnett, C.; Postelnicu, R.; Wang, C.; Banakis, S.; Pérez-Pérez, L.; Shen, G.; Jour, G.; Meyn, P.; Carpenito, J.; Liu, X.; Ji, K.; Collazo, D.; Labarbiera, A.; Amoroso, N.; Brosnahan, S.; Mukherjee, V.; Kaufman, D.; Bakker, J.; Lubinsky, A.; Pradhan, D.; Serman, D. H.; Weiden, M.; Heguy, A.; Evans, L.; Uyeki, T. M.; Clemente, J. C.; de Wit, E.; Schmidt, A. M.; Shopsis, B.; Desvignes, L.; Wang, C.; Li, H.; Zhang, B.; Forst, C. V.; Koide, S.; Stapleford, K. A.; Khanna, K. M.; Ghedin, E.; Segal, L. N. Microbial signatures in the lower airways of mechanically ventilated COVID-19 patients associated with poor clinical outcome. *Nat. Microbiol.* **2021**, *6* (10), 1245–1258.

(88) Wang, S.; Qiu, Z.; Hou, Y.; Deng, X.; Xu, W.; Zheng, T.; Wu, P.; Xie, S.; Bian, W.; Zhang, C.; Sun, Z.; Liu, K.; Shan, C.; Lin, A.; Jiang, S.; Xie, Y.; Zhou, Q.; Lu, L.; Huang, J.; Li, X. AXL is a candidate receptor for SARS-CoV-2 that promotes infection of pulmonary and bronchial epithelial cells. *Cell Res.* **2021**, *31* (2), 126–140.

(89) Rajah, M. M.; Hubert, M.; Bishop, E.; Saunders, N.; Robinot, R.; Grzelak, L.; Planas, D.; Dufloo, J.; Gellenoncourt, S.; Bongers, A.; Zivaljic, M.; Planchais, C.; Guivel-Benhassine, F.; Porrot, F.; Mouquet, H.; Chakrabarti, L. A.; Buchrieser, J.; Schwartz, O. SARS-CoV-2 Alpha, Beta, and Delta variants display enhanced Spike-mediated syncytia formation. *EMBO J.* **2021**, *40* (24), No. e108944.

(90) Dittmar, M.; Lee, J. S.; Whig, K.; Segrist, E.; Li, M.; Kamalia, B.; Castellana, L.; Ayyanathan, K.; Cárdenas-Díaz, F. L.; Morrissey, E. E.; Truitt, R.; Yang, W.; Jurado, K.; Samby, K.; Ramage, H.; Schultz, D. C.; Cherry, S. Drug repurposing screens reveal cell-type-specific entry pathways and FDA-approved drugs active against SARS-Cov-2. *Cell reports* **2021**, *35* (1), No. 108959.

(91) Yu, J. Organoids: a new model for SARS-CoV-2 translational research. *International. Journal of Stem Cells* **2021**, *14* (2), 138–149.